

UNCLASSIFIED

AD NUMBER: AD0806963

LIMITATION CHANGES

TO:

Approved for public release; distribution is unlimited.

FROM:

Distribution authorized to U.S. Gov't. agencies and their contractors; Administrative/Operational Use; 31 OCT 1966. Other requests shall be referred to Office of Naval Research, Arlington, VA 22203.

AUTHORITY

ONR ltr dtd 9 Nov 1973

THIS PAGE IS UNCLASSIFIED

INVESTIGATIONS ON THE DIRECT CONVERSION OF NUCLEAR
FISSION ENERGY TO ELECTRICAL ENERGY IN A PLASMA DIODE

ANNUAL REPORT

for

Nonr-3109(00)

October 31, 1966

RESEARCH LABORATORIES
GENERAL MOTORS CORPORATION
Warren, Michigan

2

INVESTIGATIONS ON THE DIRECT CONVERSION OF NUCLEAR
FISSION ENERGY TO ELECTRICAL ENERGY IN A PLASMA DIODE

ANNUAL REPORT

for

Nonr-3109(00)

OCTOBER 31, 1966

RESEARCH LABORATORIES
GENERAL MOTORS CORPORATION
WARREN, MICHIGAN

OFFICE OF NAVAL RESEARCH

Contract Nonr-3109(00)

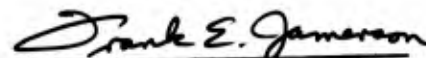
Investigations on the Direct Conversion of Nuclear
Fission Energy to Electrical Energy in a Plasma Diode

Report No. 7

Authors

Charles B. Leffert

David B. Rees



Frank E. Jamerson
Project Supervisor

Report for Period November 1, 1965 to October 31, 1966

Research Laboratories, General Motors Corporation
Warren, Michigan

Reproduction in whole or in part is permitted for any
purpose of the United States Government

This report has been prepared under Contract
Nonr-3109(00) for the Office of Naval Research and
technically supervised by Commander William F. Diehl
and Dr. Ralph Roberts.

ABSTRACT

Inpile microwave measurements of electron density in neon-argon and argon-cesium plasmas generated by fission fragments are compared with values of electron density predicted from a reaction kinetics theory. The main purpose of the comparison is to assess the validity of a theory designed to describe the dominant production and loss processes in noble gas-cesium thermionic converters over a wide range of conditions. For the neon-argon system the measured and predicted values were in good agreement; the highest electron density was $1.0 \times 10^{12} \text{ cm}^{-3}$ at full reactor power ($\phi = 1.44 \times 10^{13} \text{ cm}^{-2} \text{ sec}^{-1}$). For the argon-cesium system the agreement between theory and experiment was less satisfactory. The highest measured electron density at full reactor power was $2.3 \times 10^{12} \text{ cm}^{-3}$ - approximately twice the computed value, and this maximum in the curve of electron density vs. the ratio of Cs/Ar occurred at a ratio ($\sim 2 \times 10^{-5}$) much lower than that predicted ($\sim 3 \times 10^{-4}$). Furthermore the electron density was found to be extremely dependent upon the temperature of the cavity walls. No satisfactory explanation has yet been found for this behavior.

Favorable electron transport properties are expected to make the fission-fragment-generated argon-cesium plasma a good candidate for use in a nuclear thermionic converter. Theoretical transport properties are reported for this plasma when the major ion loss mechanism is ambipolar diffusion to the thermionic diode electrodes. The theoretical model is being expanded to include volume loss of the ions.

TABLE OF CONTENTS

	<u>Page</u>
ABSTRACT	i
INTRODUCTION	1
OBJECTIVES	1
CONCLUSIONS	2
FUTURE PLANS	3
REFERENCES	4
ACKNOWLEDGMENTS	4
INVESTIGATIONS:	
<u>SECTION</u>	
A Inpile Microwave Measurements of Electron Density in Argon-Cesium and Neon-Argon Plasmas, C. B. Leffert and D. B. Rees	36 pages
B Electron Transport in a Diffusion Controlled Plasma: Description of Computer Program and Parametric Studies, <i>C. B. Leffert</i>	32 pages
PUBLICATIONS	1 page
DISTRIBUTION	5 pages

INVESTIGATIONS ON THE DIRECT CONVERSION OF NUCLEAR FISSION ENERGY TO ELECTRICAL ENERGY IN A PLASMA DIODE

INTRODUCTION

The analysis of reaction kinetics and electron transport in a noble-gas plasma generated by fission fragment ionization has been continued. These studies evaluate such a plasma for application to a nuclear thermionic energy converter.

The rate at which fission fragments produce ions in noble gases⁽¹⁾ has been used in reaction kinetics studies to predict the steady-state electron density produced in both a neon-argon and an argon-cesium plasma.⁽²⁾ In the previous reporting period,⁽²⁾ the transport of electrons across a fission-fragment-generated plasma was considered for a plasma controlled by diffusion loss of the ions, and the description of an inpile device was presented for the measurement of the electron transport properties of such a plasma.

In this report we present first the experimental results of inpile microwave experiments to measure the electron density produced in both neon-argon and argon-cesium plasmas. These results are compared with the values predicted by the reaction kinetics theory. In the second section we present the results of parametric studies on electron transport in a diffusion controlled plasma. An initial transport device was operated inpile but the results to date are preliminary.

OBJECTIVES

The objectives initially set for the current reporting period were:

1. Continue microwave measurements inpile to determine experimentally the electron density generated by fission fragments in the Ne-Ar and Ar-Cs plasmas.
2. Compare measurements of electron density with predictions of the reaction kinetics analysis under various conditions.

3. Operate inpile thermionic diodes incorporating the BaO-UO₂-W emitter with argon-cesium and neon-argon fillings to study the electron transport through the fission-fragment-generated plasma.
4. Extend theoretical work on electron transport through noble-gas plasmas to include volume loss processes which are both linear and quadratic in electron density.

CONCLUSIONS

1. The values of electron density in the neon-argon plasma (90 torr neon, 10^{-4} Ne/Ar) as measured with the resonant microwave cavity were in good agreement with the values predicted by the reaction kinetics theory.
2. The highest measured electron density in the neon-argon plasma was $1.0 \times 10^{12} \text{ cm}^{-3}$ at full reactor power (2 MW) and $\phi = 1.44 \times 10^{13} \text{ cm}^{-2} \text{ sec}^{-1}$.
3. Variation in the intensity of the microwave signal to the cavity (Ne-Ar) produced little effect on the resonant frequency shift since the cavity was greatly undercoupled to the waveguide at the higher electron densities where some effect might be expected.
4. Variation in the cavity wall temperatures (and therefore gas temperatures) also had little effect on the electron density for Ne-Ar. A much larger variation was predicted by the reaction kinetics code. However at the present time the computations include the temperature dependence of only two (diffusion and collisional radiative recombination) of the many processes involved. The temperature dependence of the other reaction rates are being studied.
5. For the argon-cesium microwave cavity (90 torr argon), a variation of Cs/Ar from 10^{-6} to 10^{-3} was obtained simply by the use of two nitrogen circulating tubes to remove the excess fission heat.
6. The highest electron density measured for Ar-Cs was $2.3 \times 10^{12} \text{ cm}^{-3}$ at full reactor power (2MW) ($\phi = 1.44 \times 10^{13} \text{ cm}^{-2} \text{ sec}^{-1}$) with Cs/Ar $\sim 2 \times 10^{-5}$.
7. The reaction kinetics theory had predicted higher maximum electron densities for Ar-Cs than for Ne-Ar and this was borne out experimentally. Even so the maximum electron density in Ar-Cs was higher than that calculated, and more importantly, it occurred at a much lower value of Cs/Ar ($\sim 2 \times 10^{-5}$) than that ($\sim 3 \times 10^{-4}$) predicted.

8. The measured electron density in Ar-Cs was extremely dependent upon the temperatures of the cavity walls. In one run an increase of only 200°C (0.017 eV) in the average wall temperature produced an order of magnitude increase in the electron density for the same corrected value of Cs/Ar ratio.
9. Explanations of this anomalous dependence of electron density upon temperature have been sought in possible surface and volume reactions not presently included in the reaction kinetics; so far none appear capable of yielding the observed temperature behavior.
10. The thermionic electron transport model with a diffusion-controlled plasma is applicable to electron densities below $2 \times 10^{12} \text{ cm}^{-3}$. Above this density, the volume ion losses become appreciable.
11. This diffusion model with a uniform volume ionization rate from fission fragments predicts considerable variation in the electron density between the emitter and collector; typically, $n_e(\text{max})/n_e(\text{min}) \sim 40$.
12. The calculated diode current was very sensitive to the ion generation rate and diode spacing as expected. For the plasma limited conditions studied, the diode current was relatively insensitive to the emitter Richardson current.

FUTURE PLANS

1. The experimental and theoretical study of reaction kinetics in argon-cesium plasmas will be continued in order to establish the nature of the observed critical dependence of electron density upon ambient gas and wall temperatures.
2. Electron transport tubes with Ar-Cs fillings will be operated to measure electron current transport as a function of electron density in the plasma as determined from the reaction kinetics study.
3. Theoretical work on electron transport will continue with the aim of developing a theory which will satisfactorily predict current-voltage characteristics and performance of argon-cesium plasma converters. The theory will be tested against the experimental results obtained with the electron transport tubes.

4. Consideration will be given to operating a transport tube with an improved collector surface in order to increase power output. Work on the influence of fission fragments on these surfaces will be initiated.

REFERENCES

1. Investigations on the Direct Conversion of Nuclear Fission Energy in a Plasma Diode, 1964 Annual Report No. 5; C. B. Leffert, D. B. Rees, and F. E. Jamerson.
2. Investigations on the Direct Conversion of Nuclear Fission Energy in a Plasma Diode, 1965 Annual Report No. 6; C. B. Leffert, D. B. Rees, and F. E. Gifford.

ACKNOWLEDGMENTS

The authors are indebted to Professor D. J. Rose of the Massachusetts Institute of Technology for his counsel during these studies and to the University of Michigan reactor staff for their assistance during the course of the experiments.

The assistance of F. W. Chapman with the microwave experiment is greatly appreciated as was the technical assistance of Messrs. R. Dusman, R. Aikin and D. Lee.

SECTION A

SECTION A

INPILE MICROWAVE MEASUREMENTS OF ELECTRON DENSITY IN NEON-ARGON AND ARGON-CESIUM PLASMAS

ABSTRACT

Inpile microwave measurements of the electron density in neon-argon plasmas have been completed and are reported together with similar measurements for argon-cesium plasmas. The plasmas were generated by fission fragment ionization of the corresponding mixed gases in a resonant microwave cavity. Experimental techniques are described and the experimental data are analyzed in terms of the reaction kinetics theory which predicts the electron density from the various computed ion source and loss rates within the plasma. For the neon-argon plasma, theory and experiment agreed. With argon-cesium, higher electron densities were found, as predicted by theory, but the predicted maximum in electron density occurred at a much lower concentration of cesium than had been calculated. Also a temperature effect was observed in argon-cesium whereby the electron density was found to increase very rapidly as the temperature of the walls of the cavity was increased from about 400 to 700°K at constant cesium concentration.

CONTENTS

ABSTRACT	i
OBJECT	1
CONCLUSIONS	1
INTRODUCTION.	2
EXPERIMENTAL METHOD	4
RESULTS	11
Electron Density in Neon-Argon Plasma	11
Electron Density in Argon-Cesium Plasma	11
Effect of Cs/Ar on Electron Density	14
Effect of $\langle T_{\text{gas}} \rangle_{\text{av}}$ on Electron Density	14
DISCUSSION OF ANOMALOUS TEMPERATURE DEPENDENCE IN Ar-Cs.	17
(a) Dependence of Cs/Ar on $\langle T_{\text{gas}} \rangle_{\text{av}}$	18
(b) Time to Reach Equilibrium	18
(c) Delayed Surface Equilibrium	19
(d) Langmuir Surface Ionization of Cesium on Cavity Walls	20
(e) Impurities	21
(f) Interaction of Surface Adsorbed Cesium Atoms with Plasma Species	22
(g) Ionization of Cesium by Argon Excited States.	24
(h) Heteronuclear Ions	25
(i) Influence of Energetic Electrons from Penning Ionization Process	27
APPENDIX A - COMPUTATION OF CS/AR FOR MICROWAVE CAVITY.	29
APPENDIX B - DIFFUSION OF CESIUM IN ARGON	31
Overall Rate Equation	33
REFERENCES	35

OBJECT

The objectives of this study were (1) to measure the electron density in a fission-fragment-generated plasma using a resonant microwave cavity and (2) to compare the measured electron density with that predicted by the reaction kinetics theory.

CONCLUSIONS

1. The measured electron densities in the neon-argon plasma agreed well with theory.
2. The variation in electron density with gas temperature was not as great as expected for neon-argon. However the temperature dependence of only the diffusion and collisional radiative recombination rates have so far been included in the theory.
3. Use of the new wide sweep K-band microwave generator permitted much more accurate measurement of the electron density and disclosed four more resonant peaks (other than TM_{020} mode) which were also used to measure the electron density.
4. Microwave measurements on the argon-cesium plasma gave higher electron densities than for neon-argon, as had been predicted by theory.
5. When the cesium concentration in the argon varied by changing the cesium bath temperature, the electron density passed through a maximum value but at a cesium concentration much lower than that predicted.
6. Another unexpected (and very probably related) phenomenon was that the electron density was very sensitive to the temperature of the cavity walls (400-700°K).
7. The logarithm of electron density varies linearly with the inverse of the average cavity temperature which yields an "activation energy" of 0.22 eV for an unspecified process.
8. Several processes additional to those included in the reaction kinetics equations have been briefly considered in an attempt to elucidate the anomalous temperature variation of electron density. These have included: (i) the time for the cesium to diffuse from the reservoir into the cavity and reach an equilibrium value; (ii) a delayed equilibrium

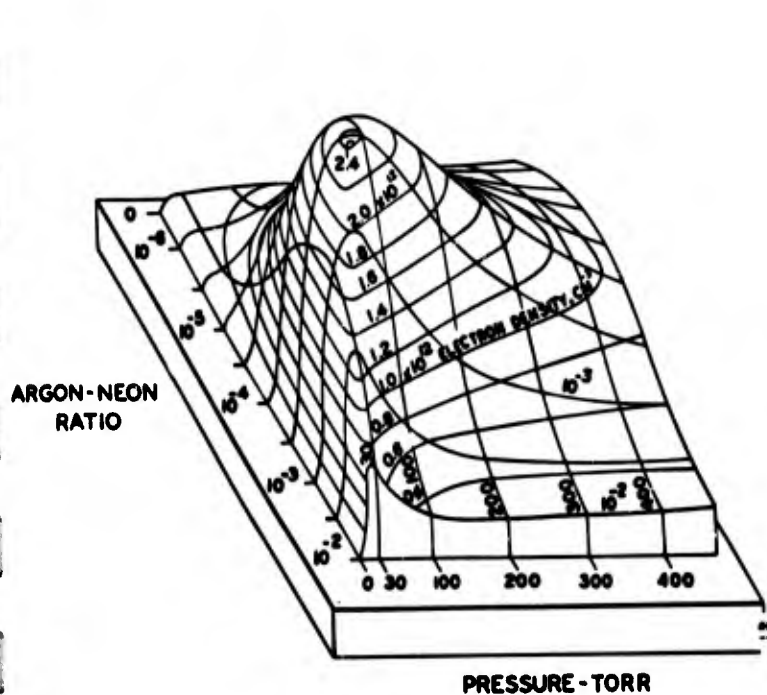
of cesium arising from surface effects; (iii) Langmuir surface ionization of cesium on the cavity walls; (iv) impurities; (v) interaction of cesium-covered surfaces with photons from the plasma; (vi) volume ionization of cesium by argon excited states which are not metastable; (vii) heteronuclear ions; and (viii) the influence of energetic electrons from the Penning ionization process. None of these processes acting independently in the present experiment appear likely to be the cause of the observed sensitive dependence of electron density upon the cavity wall temperature.

9. A 46 hour run with the Ar-Cs cavity at high temperature and high electron density showed no degradation of electron density with time.

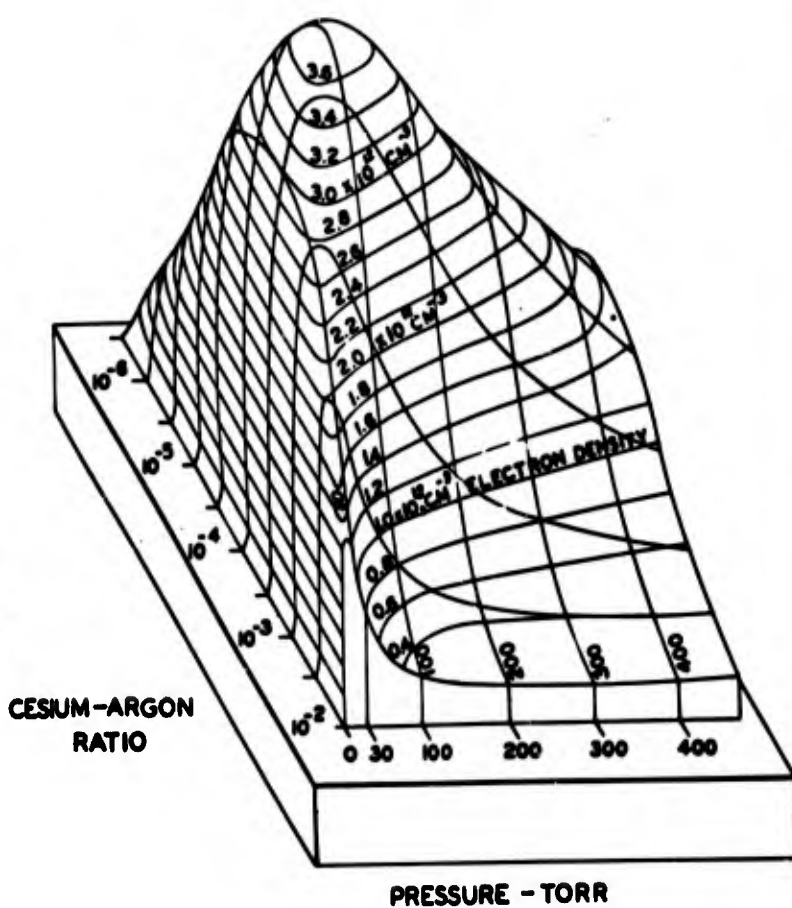
INTRODUCTION

The noble gas thermionic converter with the plasma generated by fission-fragment ionization of the gas has been described⁽¹⁾ and theoretical and experimental studies on the ion generation rate in such plasmas have been reported.⁽²⁾ The reaction kinetics analysis of mixed-gas plasmas and preliminary results of electron density measurements in Ne-Ar were presented at the San Diego meeting;⁽³⁾ also a brief report of similar measurements for Ar-Cs has appeared recently.⁽⁴⁾

In our theoretical studies of the reaction kinetics of Penning-type binary gas systems⁽¹³⁾ we showed that considerable enhancement of the electron number density over that for pure gases could be expected by the proper selection of the conditions that (1) maximize the ionization of the trace gas atoms by metastable excited atoms of the major gas species (Penning reaction) and at the same time (2) minimize the loss rate of the trace gas ion. Reaction rate equations for the atomic and molecular ions of both species and the metastable atoms of the major species in the plasma were solved for the steady state with a computer to find the influence of the gas pressure and composition on the electron density. The results of these computations are reproduced here in Fig. 1 for neon-argon and for the argon-cesium system. The gas temperature (1300°K) and neutron flux ($1 \times 10^{13} \text{ cm}^{-2} \text{ sec}^{-1}$) are typical conditions for our thermionic converter operating in a research reactor (2 mW). In both systems a singular electron number density maximum was found at a pressure of about 90 torr and at a trace gas concentration of about 0.01%. It was to verify this predicted behavior that the inpile microwave measurements of electron density were performed.



(a)



(b)

Fig. 1. Contour map showing the singular electron number-density maximum in a 1300°K fission-fragment-generated plasma of neon-argon (a) and argon-cesium (b). The diffusion length of the container is 1.6 mm and the neutron flux is $1 \times 10^{13} \text{ cm}^{-2} \text{ sec}^{-1}$.

EXPERIMENTAL METHOD

The method of measuring the electron density (n_e) in a plasma from the shift $\{\Delta\omega\}$ in the resonant angular frequency of a microwave cavity is well known.^(5,6) $\Delta\omega$ is related to n_e by

$$\Delta\omega = \frac{1}{2\omega} \left[\frac{1}{1 + (\nu/\omega)^2} \right] \frac{e^2}{\epsilon_0 m} V \frac{\int n_e E^2 dV}{\int E^2 dV} \quad (1)$$

where E is the electric field within the volume V of the cavity, ω is the frequency of the empty cavity, e and m are the electronic charge and mass of the electrons, ϵ_0 is the permittivity of free space and ν is the collision frequency of the electrons. The fission-fragment ion generation rate is fairly uniform⁽²⁾ and we expect to operate in the regime where the volume losses predominate. Thus the electron density is assumed to be uniform over V and the integrals cancel in Eq.1 (after removal of n_e). We will operate at pressures ~ 100 torr where the collision frequency is of order $\nu \sim 5 \times 10^9 \text{ sec}^{-1}$. The resonant angular frequency will be $\sim 1.5 \times 10^{11} \text{ sec}^{-1}$ (K-band microwaves) so the factor in brackets in Eq.1 becomes unity. With these simplifications, Eq.1 reduces to

$$n_e (\text{cm}^{-3}) = \frac{f_o}{4 \times 10^7} \Delta f (\text{GHz}) \quad (2)$$

where f_o is the resonant frequency of the empty cavity in GHz.

In order that the microwave cavity could be mounted inside a tube (i.d. = 2-3/4 in.) which was to fit a standard fuel element position in the core of a swimming pool-type research reactor, we selected the TM_{020} mode⁽⁶⁾ for a right circular cylinder for the cavity geometry as shown in Fig. 2. The general method of cavity construction was similar to that used earlier⁽¹⁾ but will be repeated both for completeness and since Fig. 2 incorporates improvements over the earlier design.⁽¹⁾

The body of the cavity was made of Kovar. The window was made of high density alumina and after coating with molybdenum-manganese it was brazed to the Kovar retainer with copper. A short section (2-1/4 in.) of stainless steel waveguide was brazed to the Kovar at the same time that the ceramic

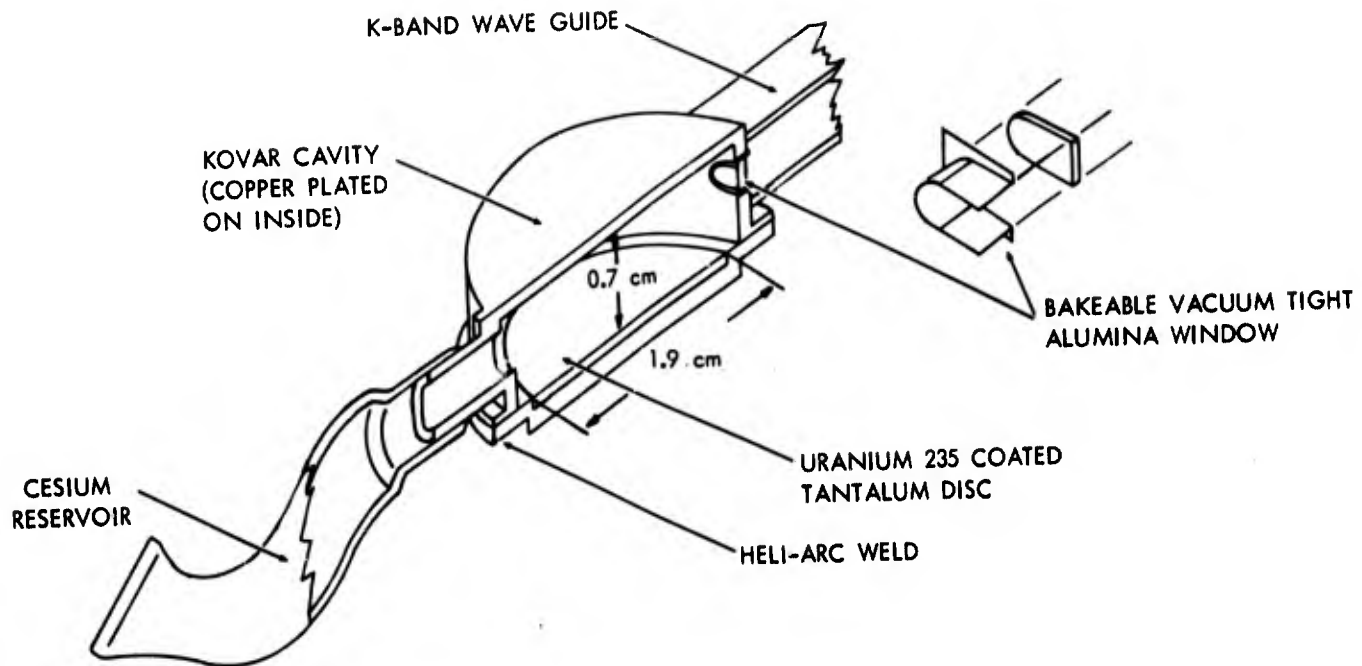


Fig. 2. Microwave cavity for Ar-Cs inpile studies. The Ne-Ar cavity was identical except for a small pump-out tubulation instead of the cesium bath.

window and retainer were brazed in place. The inside of the cavity (less the Kovar cap) was electroplated with copper (~ 0.004 in.). Two tantalum discs (0.010 in.) were brazed to the Kovar cap with copper and the U-235 foil (0.001 in.) was brazed to the top tantalum disc with nickel. After the Kovar cap was spot-welded in place the periphery was heliarc-welded to complete the tube construction. This cap design afforded better electrical contact and gave better signal characteristics than the earlier design.⁽¹⁾

The TM_{020} mode for a right circular cylinder cavity (Fig. 2) was selected with $f_0 = 23.1$ GHz (K-band) so that an electron density of $\sim 5 \times 10^{11} \text{ cm}^{-3}$ would yield a frequency shift $\Delta f \sim 1$ GHz. This mode fixed the cavity inside diameter at $d = 2.272$ cm but the height was still arbitrary. For the two cavities discussed here the height was $h = 0.7$ cm (in the first inpile run $h = 0.5$ cm⁽¹⁾).

In the construction of the first Ne-Ar microwave cavity considerable trouble was experienced in obtaining a vacuum-tight seal between the ceramic microwave window and the cavity.⁽¹⁾ This problem was solved by first bonding the ceramic to a thin walled Kovar tube and then brazing the Kovar tube to the cavity wall (Fig. 2). Also the circular ceramic window for the first cavity was made as large in diameter as possible consistent with K-band

waveguide but the empty cavity was undercoupled nevertheless and severe loss of signal resolution developed as the plasma density increased (plasma decreases the coupling).⁽⁵⁾ To solve this problem, for the cavities reported here, the ceramic window was changed from a circular to oval shape in order to give a larger cross sectional area. This change gave an overcoupled empty cavity and better signal resolution with a plasma.

After construction, the cavity was baked at 600°C on an ultra-high vacuum system* and evacuated to a pressure of 6×10^{-9} torr. Then, under vacuum, the five cesium chromate pellets contained in a glass side-arm were carefully flashed inductively and the cesium subsequently flash distilled into the cesium reservoir (Fig. 3) maintained as a cold region. A system vacuum (non-condensibles) of less than 10^{-8} torr was recorded after completing this operation. The manifold was isolated from the vacuum system and Airco reagent grade argon was then slowly admitted at room temperature to a pressure of 90 torr (recorded using a bakeable glass spiral gauge) and the cavity was pinched off the system at the copper pump-out tubulation. Finally the copper pinch-off was checked for leaks.

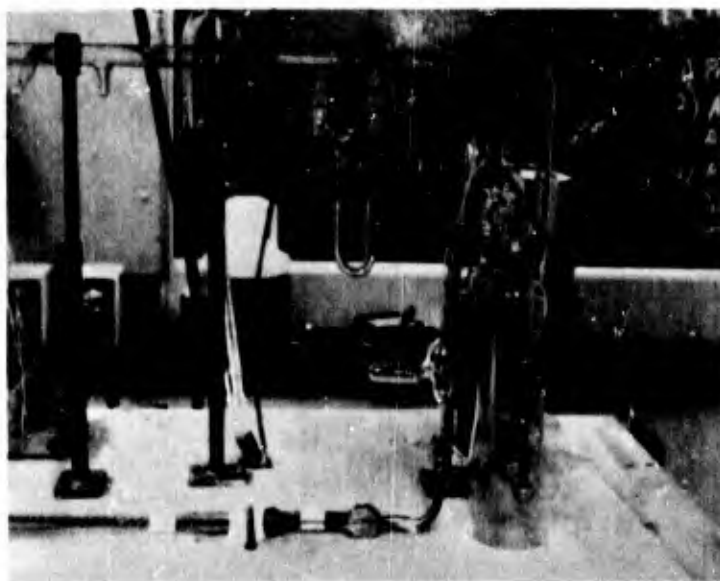


Fig. 3. Microwave cavity attached to the ultra-high vacuum system.

* A separate oven was placed over the cavity during bake-out in order to raise its temperature to 600°C compared with the 450°C bake-out temperature for the remainder of the ultra-high vacuum system.

A photograph of the finished assembly including the coolant tubes and thermocouples is shown in Fig. 4.

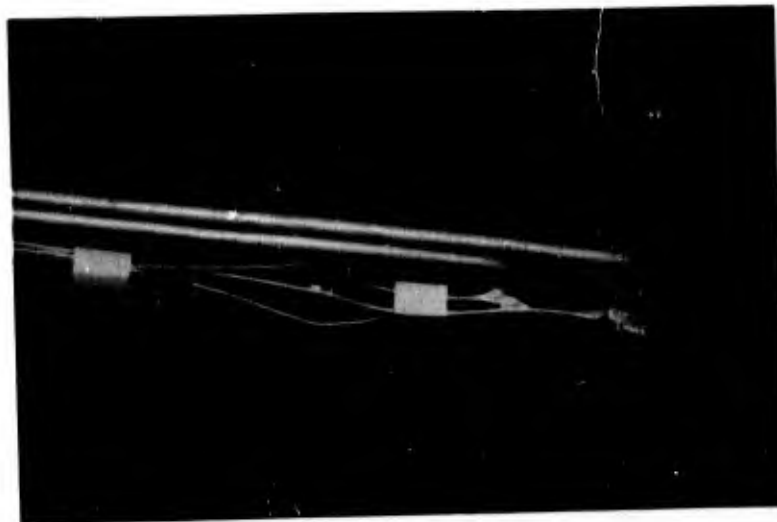


Fig. 4. Microwave cavity assembly ready for insertion into the 3 in. o.d. x 4 ft long containment can.

The circuit for the measurement of the cavity resonant frequency is shown in Fig. 5.

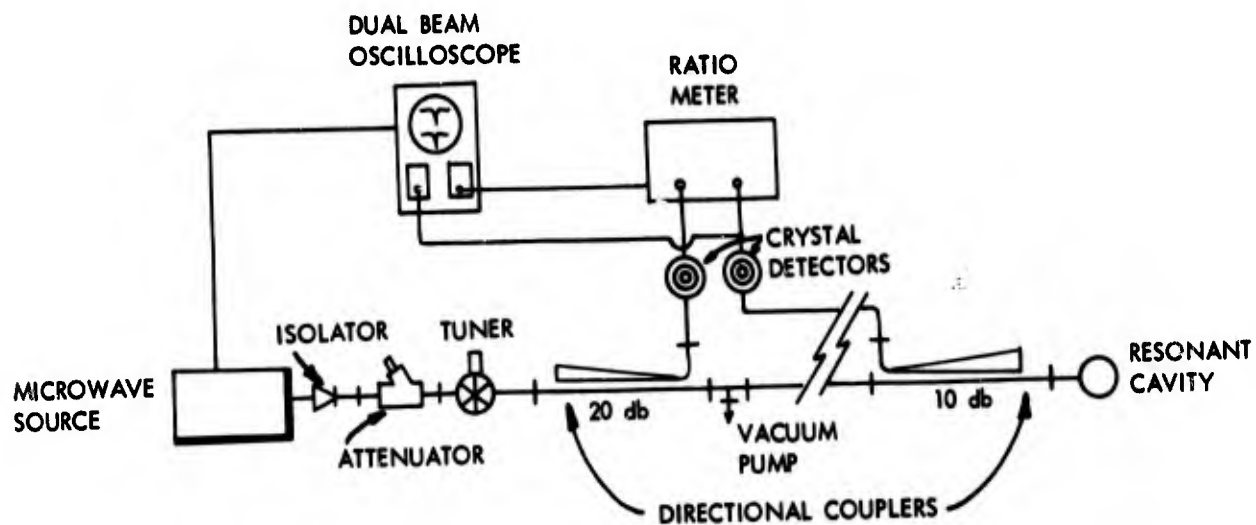


Fig. 5. Microwave circuit for measurement of cavity resonant frequency.

Additions to the circuit described previously⁽¹⁾ include a new wide sweep K-band microwave generator (H.P.696A), a ratiometer (H.P.210A) for direct measurement of the VSWR and display on the oscilloscope, new wide band crystal detectors (H.P.422A) and a precision attenuator to permit study of the shift of the cavity resonant frequency (plasma conditions) with variation of the incident microwave power input.

During the inpile runs on these cavities with the new wide sweep microwave generator we discovered other resonances as shown in Fig. 6.



Fig. 6. Typical signal output versus frequency sweep (horizontal scale is 22.0 to 26.5 GHz) at operating conditions ($n_e \sim 7 \times 10^{11} \text{ cm}^{-3}$). The upper beam is the reflected signal crystal diode output ($-V$) and the lower beam is the ratiometer output ($+V$). The five resonant peaks are identified in Table I.

Computations for both the TE and TM modes identified these resonances as shown in Table I. Best agreement between computed and measured mode frequencies was obtained by assuming $d=2.287$ cm and $h=0.693$ cm. These values are consistent since the originally measured $d=2.272$ cm should increase by thermal expansion inpile and h (0.7) cm could either decrease or increase dependent on the accuracy of the Kovar cap assembly.

TABLE I. Observed resonances.

Mode	f_o (computed) GHz	f_o (measured) (empty cavity)GHz	Position in Fig. 6, cm
TM ₂₁₀	21.44	---	2.0
TE ₁₁₁	22.96	22.91	5.2
TM ₀₂₀	23.05	23.10	5.7
TM ₀₁₁	23.85	23.86	6.8
TE ₂₁₁	25.11	25.12	9.3

The microwave cavity was supported by the end of the waveguide inside an aluminum containment tube as shown in Ref. 1 (for the first inpile microwave on neon-argon).⁽¹⁾ The same method was used for the neon-argon inpile run to be described here but in addition a 1/4 in. aluminum tube was installed so that it terminated very close to the outside surface of the uranium wall. This was used to direct a cooling stream of N₂ against the uranium wall thereby enabling us some control of the wall temperature (about 80 watts of heat are liberated in the 1 mil uranium foil at full reactor power of 2 mW). For the Ar-Cs cavity, a second N₂ gas coolant stream was directed against the cesium bath in order to control separately the temperature of the cesium bath. Thermocouples were attached to the uranium and Kovar sides of the microwave cavity and also to the cesium bath.

A photograph of the operation at the University of Michigan research reactor is shown in Fig. 7. The microwave generator is on the wooden platform in the center of the reactor bridge and the waveguide connects to the aluminum containment can in the reactor core. The ratiometer is at the right of the bridge (above grill) and the oscilloscope is at the extreme right of the picture. The aluminum containment can containing the cavity, the microwave generator and the interconnecting plumbing were all supported from one screw jack so that the cavity could be positioned vertically in the core to vary the neutron flux independent of the reactor power.

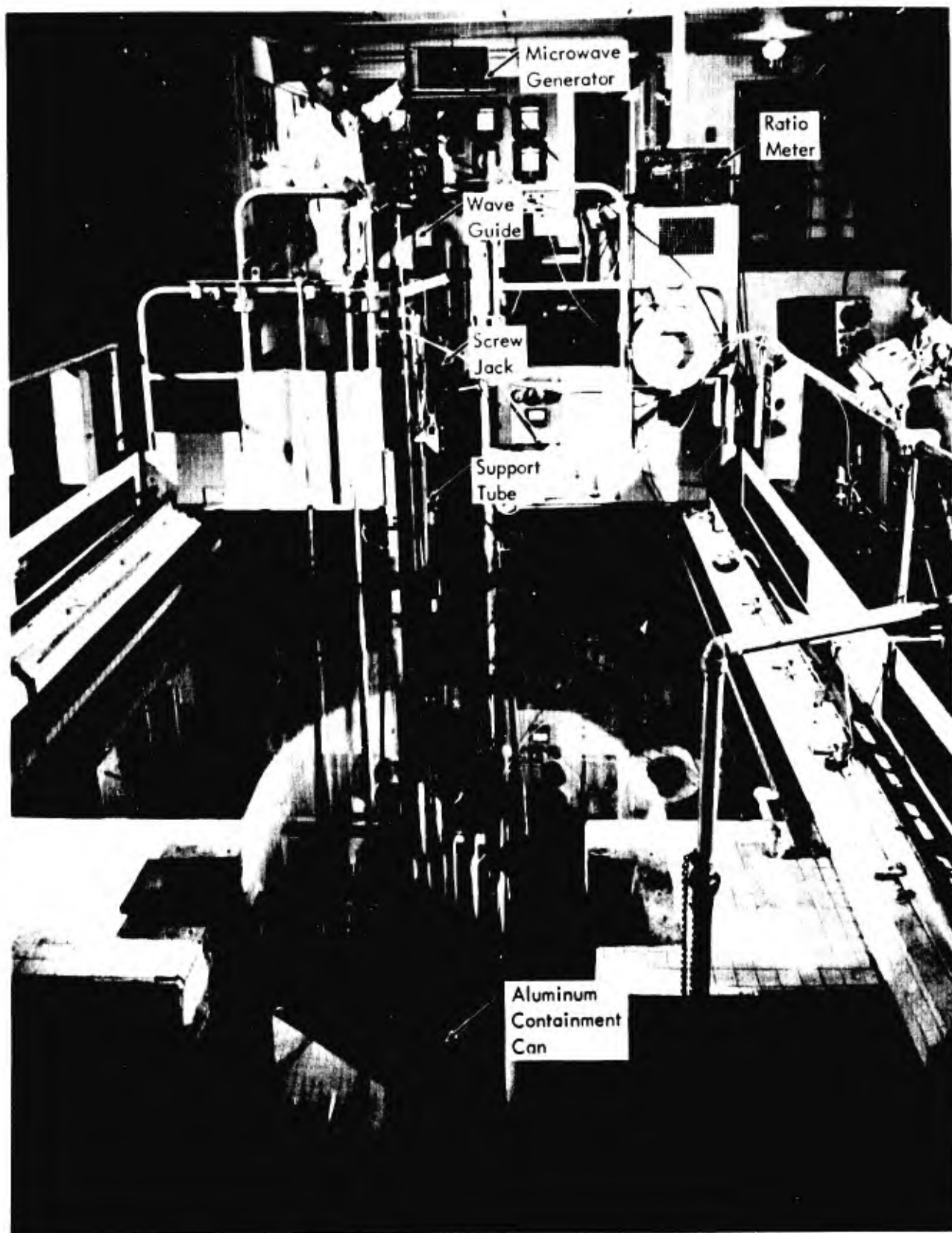


Fig. 7. Operating experimental arrangement at the University of Michigan research reactor.

RESULTS

Presented in this section are the data from the second neon-argon microwave cavity and the data from the argon-cesium microwave cavity.

Electron Density in Neon-Argon Plasma

In the first run with this cavity at low reactor power the shift in frequency indicated electron densities which were very low — in fact they were less than that predicted for pure neon. However as the run progressed the electron density increased with time and finally stabilized at electron densities consistent with theory. This behavior has been attributed to clean-up (probably by the uranium) of a contaminant (possibly O_2) which was liberated at the beginning of the run from the cavity walls by the nuclear radiations. During subsequent runs there was an additional small increase of electron density with time which may be due to a redistribution of the uranium on the foil surface (see discussion of argon-cesium data).

The data from the last run are shown in Fig. 8 where the electron density is plotted against the neutron flux. The solid curves were computed from our reaction kinetics theory and no adjustable parameters are involved. Curves were computed for 10^{-4} Ar/Ne at 90 torr for gas temperatures of 300°K and 600°K. The only temperature dependence which we have built into the reaction rates to date is that for diffusion ($\propto T$) and that for collisional radiative recombination ($\propto T^{-9/2}$). Also shown for comparison is a computed curve (dashed) for pure neon at 90 torr and 300°K.

The experimental data are shown as points. With only nuclear heating of the cavity, there was a gradual increase of the average cavity temperature ($= \langle T_{Gas} \rangle_{av}$) with increasing neutron flux from about 320°K at $\phi \approx 10^{10} \text{ cm}^{-2} \text{ sec}^{-1}$ to about 500°K at $\phi \approx 10^{13} \text{ cm}^{-2} \text{ sec}^{-1}$. The highest electron density was $1.0 \times 10^{12} \text{ cm}^{-3}$ at full reactor power (2 mW). The agreement of experiment with theory is considered good. The one experimental point reported last year^(1,3) for the same gas mixture but at a pressure of 140 torr was $n_e = 5.3 \times 10^{11} \text{ cm}^{-3}$ at $\phi = 4 \times 10^{12} \text{ cm}^{-2} \text{ sec}^{-1}$ and $\langle T_{Gas} \rangle_{av} = 551^\circ \text{K}$.

At low electron densities ($< 10^{10} \text{ cm}^{-3}$) the theory predicts that the electron density will decrease with increasing gas temperature because of increased diffusion losses while at higher electron densities, where the collisional-radiative recombination rate is the predominant loss, the electron density

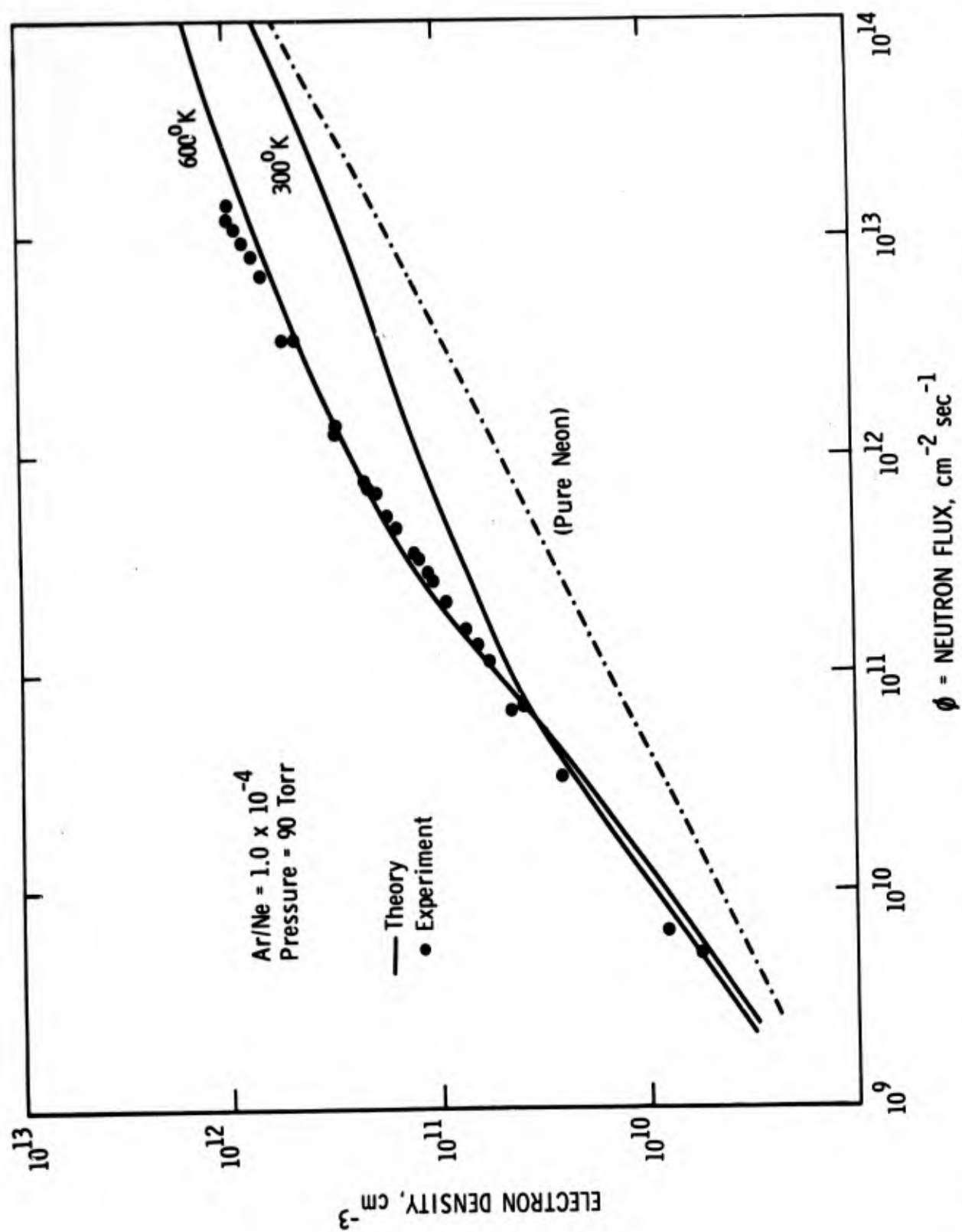


Fig. 8. Comparison of experimental and theoretical values of electron density versus neutron flux for neon-argon. The theoretical curves are for constant temperatures of 300°K and 600°K.

increases with the gas temperature. By increasing the microwave power, which heats the electrons (and thereby the gas), the electron density in general followed the direction predicted by theory. However at high electron densities the coupling of the cavity to the waveguide had become so small that variation of the power level of the incident signal made only a small change in the electron density.

The variation of electron density with the cooling gas flow to the cavity (and thus the gas temperature) also in general followed the direction predicted by theory but the magnitude of the change, particularly at high electron densities, was very much less than that predicted by the theory. A study is under way to include the temperature dependence of the other potentially important rates in the reaction kinetics code since there may be compensating processes.

Electron Density in an Argon-Cesium Plasma

The additional parameter that could be varied with the argon-cesium cavity was the ratio of the density of the minor to major gas species. This tube was filled to 90 torr of argon and the cesium to argon atom ratio (Cs/Ar) could be varied inpile from 10^{-6} to 10^{-3} by adjusting the temperature of the cesium reservoir. In the first reactor run a maximum in the electron density was obtained at a Cs/Ar very nearly at the ratio predicted by theory. However, later runs showed that the electron density was strongly dependent upon the temperature of the cavity walls, and the wall temperatures had not been held constant during the first run. The first runs were repeated with care to maintain the average cavity wall temperature constant. Since only one wall (uranium) of the cavity was cooled with gas, it was not possible to maintain independent temperature control of both walls of the cavity. The gas temperature effects to be discussed might be due to surface phenomena on the inside walls of the cavity and/or collisional processes in the plasma. Nevertheless we define the average gas temperature to be

$$\langle T_{\text{gas}} \rangle_{\text{av}} = 1/2 [T(\text{uranium electrode}) + T(\text{Kovar electrode})] \quad (3)$$

and reference to the "effect of $\langle T_{\text{gas}} \rangle_{\text{av}}$ " should be understood to include possible surface reactions.

Effect of Cs/Ar on Electron Density - To find the effect of Cs/Ar on the electron density (n_e) at constant gas temperature two inpile runs were made: the first at a neutron flux $\phi=0.72 \times 10^{13} \text{ cm}^{-2} \text{ sec}^{-1}$ and $\langle T_{\text{gas}} \rangle = 576^\circ \text{K}$, and the second at $\phi=1.44 \times 10^{13} \text{ cm}^{-2} \text{ sec}^{-1}$ and $\langle T_{\text{gas}} \rangle = 644^\circ \text{K}$. The data are plotted in Fig. 9 together with the curves predicted from the reaction kinetics code for the same conditions.

The electron density maxima in the experimental curves occur at Cs/Ar ratios considerably lower than predicted by theory. The maxima are predicted for $\text{Cs/Ar} \approx 3 \times 10^{-4}$ while the experimental maxima are at an order-of-magnitude smaller. For the lower experimental curve of Fig. 9, the electron density at the maximum is about equal to that predicted; however for the higher experimental curve the measured maximum electron density is about twice that predicted. The difference in electron density of the two theoretical curves is due mostly to the difference in neutron flux and the large difference in electron density of the two experimental curves is evidence of an anomaly in the dependence of electron density on $\langle T_{\text{gas}} \rangle_{\text{av}}$.

Effect of $\langle T_{\text{gas}} \rangle_{\text{av}}$ on Electron Density - To establish the dependence of the electron density on the average gas temperature (and/or cavity wall temperature), three runs were made at different constant values of Cs/Ar in which the cooling gas flow rate to the uranium wall of the cavity was varied, and the cooling gas flow to the cesium reservoir adjusted to obtain the desired temperature distribution for a constant Cs/Ar ratio in the cavity. In order to span a significant temperature range for each run it was also necessary to make the runs at different values of the neutron flux. The results of these measurements are shown in Fig. 10 together with the predicted curves.

In all three runs the electron density increased more rapidly with temperature than that predicted. The increase in n_e with $\langle T_{\text{gas}} \rangle_{\text{av}}$ was greatest at the lower cesium concentrations of $\text{Cs/Ar} = 1.0 \times 10^{-6}$ and 5.6×10^{-5} . Also, at these lower cesium concentrations the measured electron density tended to be higher than the predicted value, while at the higher cesium concentration ($\text{Cs/Ar} = 10^{-3}$) the measured electron density was less than that predicted. Even at the lowest cesium concentration ($\text{Cs/Ar} = 10^{-6}$), however, the measured and theoretical curves cross at an average gas temperature of 410°K . This dependence of the measured electron density on the average gas temperature (and/or

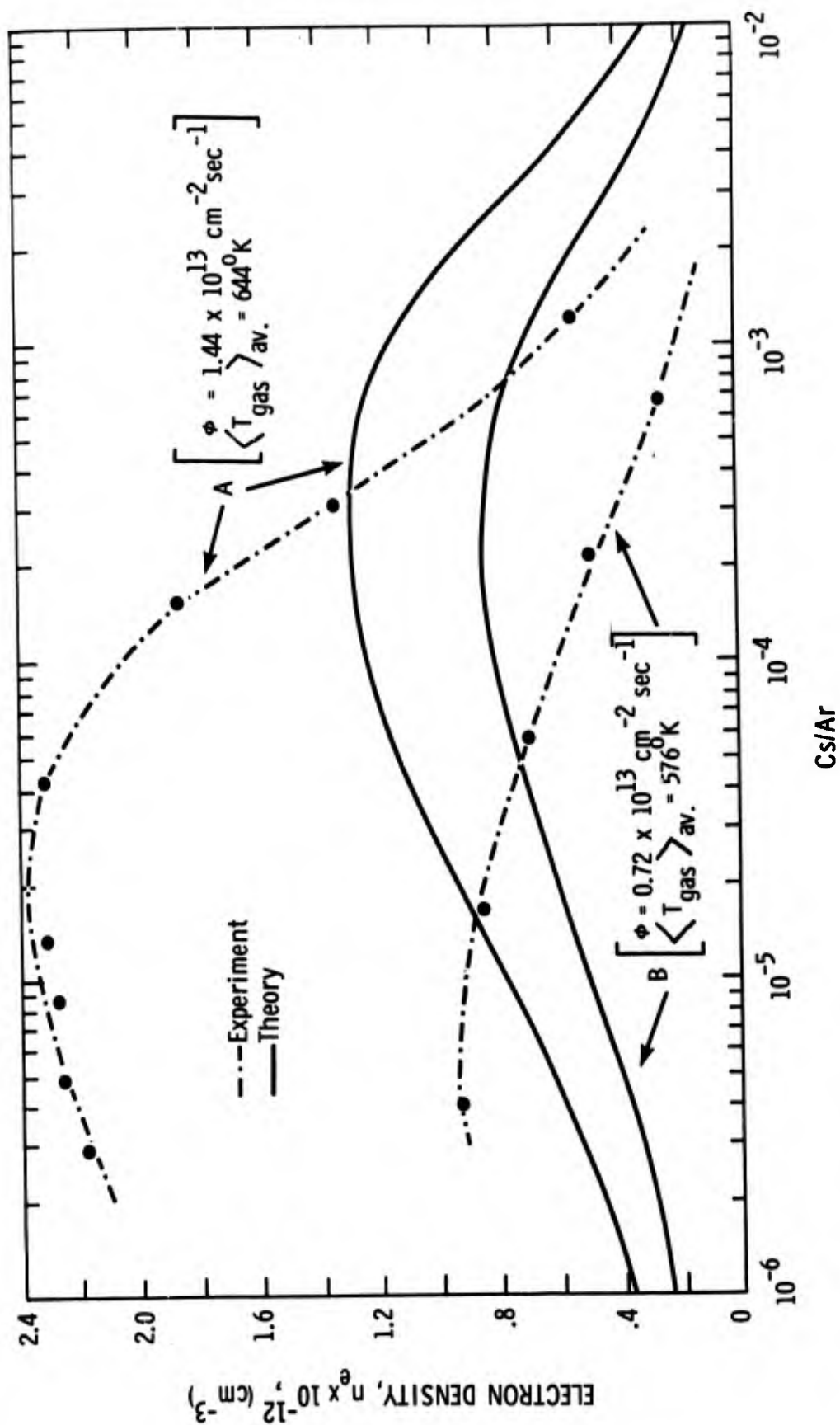


Fig. 9. Comparison of experimental and theoretical values of electron density versus Cs/Ar ratio for two constant values of neutron flux and average gas temperature.

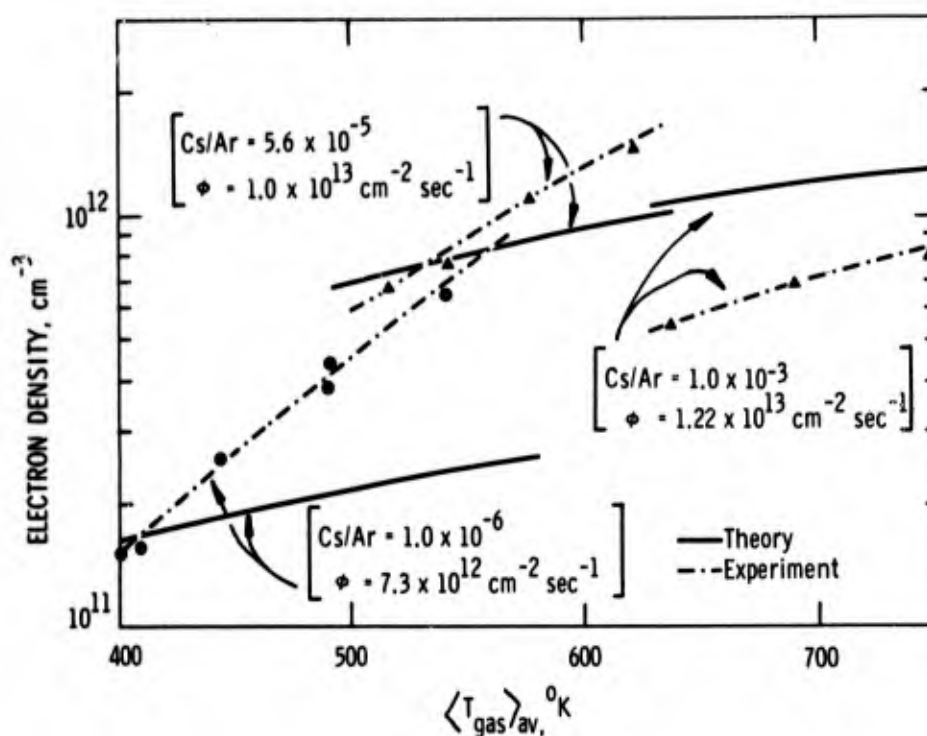


Fig. 10. Variation of electron density with average gas temperature. The theoretical and experimental values are compared under three separate conditions of constant Cs/Ar ratio and neutron flux.

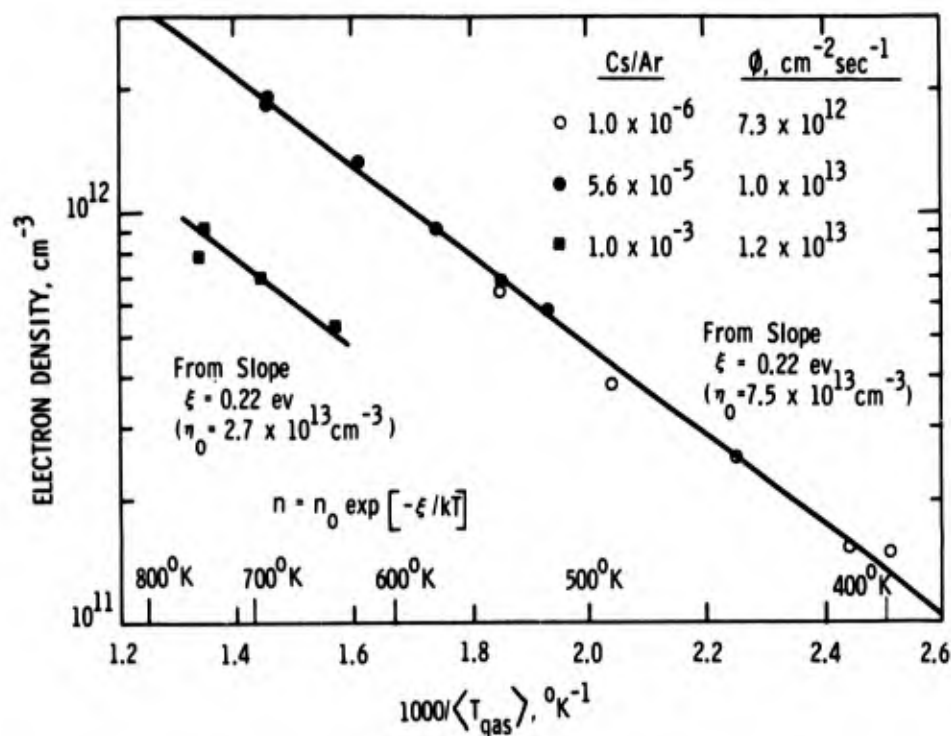


Fig. 11. Experimental values of electron density versus reciprocal values of average gas temperature. All the data are consistent with an "activation energy" of 0.22 eV represented by the slope of the solid lines.

cavity wall temperature) is extremely large; e.g., for the run with $Cs/Ar=10^{-6}$, an increase in $\langle T_{gas} \rangle_{av}$ of only $200^\circ C (=0.017 \text{ eV})$ produced an order-of-magnitude increase in the electron density. In Fig. 11 the dependence of the electron density on temperature is shown as a function of the reciprocal of the average gas temperature, $\langle T_{gas} \rangle_{av}^{-1}$. All of the data from the runs at the three different Cs/Ar ratios fit the exponential function

$$n = n_0 \exp \left[- \xi / (kT/e) \right] \quad (4)$$

with an "activation energy" $\xi = 0.22 \text{ eV}$. The significance of ξ will be discussed later.

The electron density computed from the present model is already strongly temperature dependent since for values of $Cs/Ar < 10^{-3}$, the predominant loss mechanism for the cesium ion (Cs^+) is the 3-body collisional-radiative recombination which varies as $T^{-9/2(1)}$. Besides the $T^{-9/2}$ dependence of this reaction, the only other temperature dependence built into the present reaction kinetics model for Ar-Cs is the variation of the diffusion coefficients with temperature. The temperature dependences of the other reactions in the model are being evaluated but individually their temperature dependence is expected to be small ($\propto T^{1/2}$). For this reason we have initially sought other explanations of this effect. These are discussed in the next section.

DISCUSSION OF ANOMALOUS TEMPERATURE DEPENDENCE IN Ar-Cs

The striking influence of small changes in the average cavity temperature upon the electron density in Ar-Cs led us first to reexamine our technique of calculating the cesium density in equilibrium with the cesium reservoir — particularly since the anomalous temperature effect had not been previously observed in the non-condensable neon-argon system. Additionally, we considered other possible processes not presently included in the reaction kinetics equations. What follows is a listing with comments on these processes, none of which acting independently appear likely to offer an explanation of the observed temperature behavior over the full range of experimental conditions. The processes discussed are: (a) Dependence of Cs/Ar on $\langle T_{gas} \rangle_{av}$

(b) Time to reach equilibrium (c) Delayed surface equilibrium (d) Langmuir surface ionization of cesium on cavity walls (e) Impurities (f) Interaction of surface adsorbed cesium atoms with plasma species (g) Ionization of cesium by argon excited states (h) Heteronuclear ions and (i) Influence of energetic electrons from Penning ionization process.

(a) Dependence of Cs/Ar on $\langle T_{\text{gas}} \rangle_{\text{av}}$ - At equilibrium the vapor pressure of the cesium in the cavity, $p(\text{Cs})$, is equal to that in the cesium reservoir and is fixed by the temperature of the cesium reservoir, $T(\text{Cs})$. However, the number density of cesium atoms in the cavity, $n_1(\text{Cs})$, is also a function of the gas temperature in the cavity. Also the number density of argon atoms in the cavity, $n_1(\text{Ar})$, is a function of $\langle T_{\text{gas}} \rangle_{\text{av}}$ as well as the initial filling pressure (p_0) since when the cavity is heated to a temperature higher than the cesium reservoir temperature some of the argon atoms are driven from the cavity into the reservoir. The equation which takes into account these effects is derived in Appendix A and is

$$\frac{\text{Cs}}{\text{Ar}} = \frac{p(\text{Cs})}{p_0} \left[\frac{195}{\langle T_{\text{gas}} \rangle_{\text{av}}} + \frac{105}{T(\text{Cs})} \right] \quad (\text{A-8})$$

(b) Time to Reach Equilibrium - A change in temperature of the cesium reservoir produces a change in vapor pressure in the reservoir. This leads to a flow of cesium between the reservoir and cavity to establish not only a new equilibrium concentration in the gas in the cavity, but also a new equilibrium surface coverage on the inside walls of the cavity. With an argon gas filling of about 100 torr, the mean free path of a cesium atom is much less than the dimensions of the reservoir, cavity or throat and therefore diffusion theory is applicable. In Appendix B a rate equation is derived for the diffusion of cesium from the reservoir to the cavity and the result is summarized here. If $n_1(\text{Cs})$ is the cesium density in the cavity and $n_2(\text{Cs})$ that above the fluid in the reservoir, we get

$$\frac{n_1(\text{Cs})}{n_2(\text{Cs})} = 1 - e^{-t/\tau} \quad (\text{B-10})$$

where time constant τ is given by

$$\tau = \frac{3(1 + K_2) n(\text{Ar}) Q_D \text{ LV}}{\bar{\mu} \sigma} \quad (\text{B-9})$$

This equation assumes that the gas and surrounding surfaces in the cavity approach their equilibrium values and that K_2 atoms of cesium are deposited on the surfaces per unit cesium atom increase in the gas. $n(\text{Ar})$ is the argon number density, Q_D is the momentum loss cross section for collisions between cesium and argon atoms at average relative velocity $\bar{\mu}$. L is the length and σ the cross sectional area of the throat and V is the volume of the cavity.

For typical conditions $\tau=0.675$ hr which means that starting from no cesium in the cavity, 90% of the equilibrium concentration would be reached in $\sim 1-1/2$ hr. After equilibrium has once been reached and conditions changed, the new equilibrium state should be reached within one hour. Our inpile experiments support this conclusion.

(c) Delayed Surface Equilibrium - The plot of the electron density versus $\langle T_{\text{gas}} \rangle_{\text{av}}$ (Fig. 11) implied a volume or surface reaction with an activation energy of $\xi=0.22$ eV. This suggested that possibly, contrary to the assumptions above, the cesium density in the cavity was not in equilibrium with that in the cesium reservoir even after time periods of about 1 hour, but instead that a temporary additional source of cesium existed on the cavity walls (e.g., note the flange on the uranium wall in Fig. 2). The release rate of this excess cesium would then depend upon the cavity wall temperatures. At the lower cesium to argon ratios this source would feed additional cesium to the gas to produce a cesium to argon ratio higher than that computed from equilibrium with the cesium reservoir temperature. This explanation therefore might account for the apparent shift of the maxima in n_e to lower Cs/Ar in Fig. 9 and also might account for the anomalous temperature dependence. On the other hand this explanation would require a means for the build-up of excess cesium on the cavity walls. Such a build-up might occur during the long down time (few weeks storage in the reactor pool) between runs inpile. It was found that cesium does build up on the inside surface of the ceramic microwave window and it requires about 1/2 hour of inpile operation at maximum cavity temperature to clear the window so that the resonant structure can be seen in the reflected signal (see Fig. 6).

In order to check the above hypothesis, an extended inpile run (46 hours) was made at constant conditions to see if such a source of cesium could be exhausted. The conditions chosen were those for the maximum

electron density (experimental) for curve A in Fig. 9 so that depletion of the source would be evidenced by a drop in the electron density as the Cs/Ar returned from the high non-equilibrium value to the lower computed (equilibrium) value. There was no decrease in electron density for the 46 hour run and it was concluded that no excess source of cesium was present.* During the run the electron density actually increased from $1.3 \times 10^{12} \text{ cm}^{-3}$ to $1.8 \times 10^{12} \text{ cm}^{-3}$. This increase was attributed to an increase in gas pressure (fission release of xenon and krypton) and/or a redistribution of the uranium-235 on the walls of the cavity. According to the Reactor Operating Staff and our neutron flux probe,⁽¹⁾ the neutron flux did not change during the run.

(d) Langmuir Surface Ionization of Cesium on Cavity Walls - Because of the low ionization potential of the cesium atom ($V_I = 3.89 \text{ eV}$), it is readily ionized on a hot, bare metallic surface particularly when the work function is greater than 3.89 eV . If such an additional source of ions occurred at the walls of the microwave cavity the rate of ionization would be dependent upon the temperature of the walls. The fraction of arriving cesium atoms that are ionized at a surface (β) is given in terms of Saha Equilibrium⁽⁷⁾

$$\beta = \frac{1}{1 + 2 \exp (V_I - \phi)/kT} \quad (5)$$

At the temperature of interest in the microwave studies ($400\text{--}700^\circ\text{K}$) the metallic surface is partially covered with cesium atoms adsorbed on the surface. This fraction of a monolayer (θ) is itself temperature dependent and, in fact, produces most of the temperature dependence in Eq.(5) at 700°K . In order to estimate the possible importance of surface ionization on the behavior of the microwave cavity it was decided to calculate the temperature the walls must assume (T') so that the surface production rate of ions would equal the volume production rate of ions. The dependence of θ on T was not known for Kovar or uranium so values for tungsten⁽⁸⁾ were used. T' should be even higher for uranium or Kovar.

For $\text{Cs/Ar} = 10^{-4}$ and an argon pressure of 90 torr $N(\text{Cs}) = 2.9 \times 10^{14} \text{ cm}^{-3}$ and the cesium arrival rate $R = N\bar{v}/4 \approx 10^{18} \text{ cm}^{-2} \text{ sec}^{-1}$. The volume production rate

* A surface deposit with lifetime > 46 hours is possible but very improbable since sufficient time has elapsed to transport about 150 monolayers of cesium to the cesium reservoir for a non-equilibrium (Cs/Ar)' of $\sim 4 \times 10^{-4}$.

of ions equals the volume ionization rate ($S \approx 10^{16}$ ions $\text{cm}^{-3}\text{sec}^{-1}$) times the cavity volume ($V = 2.83 \text{ cm}^3$) and the surface production rate equals β times the cesium arrival rate ($R = 10^{18} \text{ cm}^{-2}\text{sec}^{-1}$) times the surface area ($A = 13.10 \text{ cm}^2$). Equating these production rates and solving for β

$$\beta = \frac{SV}{RA} = 2.2 \times 10^{-3}.$$

Now solving Eq.(5) for T gives $T = 1450^\circ\text{K}$. This is considerably higher than the maximum temperature measured so it was concluded that Langmuir surface ionization of cesium was negligible.

The uranium foil is heated by nuclear fission. Most of the fission energy is deposited along the fragment track in electronic collisions and it might be supposed that very hot spots would be produced where the fragment leaves the uranium surface. However, investigations⁽⁹⁾ have shown that most of the energy can be dissipated by the lattice structure in very short times of order 10^{-11} sec. Therefore these local spots would not have sufficient lifetime and size to produce appreciable local Langmuir surface ionization.

(e) Impurities - Unknown impurities are often invoked as the cause of unpredictable plasma behavior. Even so, we do not favor such a cause in the present experiments for the following reasons.

Stringent conditions of cleanliness were observed during fabrication and processing of the Ar-Cs cavity. For example, during bake-out the cavity was heated to 600°C and evacuated to 6×10^{-9} torr. The cesium was carefully flash-distilled into the cavity reservoir under high vacuum and then filled with Airco reagent grade argon. The final cavity pinch-off was checked for leaks using a high-sensitivity mass-spectrometer leak detector.

Inpile, fission products released from the uranium surface are a source of impurity. The dominant gaseous products are xenon and krypton which because of their nature and release rate cannot measurably affect the electron density in the Ar-Cs plasma over the time scale of the present experiment. We can conceive of other more deleterious impurities such as oxygen being released inpile, possibly arising from fission-fragment bombardment of oxide-coated surfaces. However, the strong gettering action of both uranium and cesium is expected to minimize the concentration of such

impurities. More importantly, our inpile experiment has yielded reproducible results from the outset and in one instance the cavity was operated continuously inpile for 46 hours (Section C) with no significant change in the temperature dependence of the electron density. This behavior is contrary to that expected from the progressive build-up of important impurities with time.

(f) Interaction of Surface Adsorbed Cesium Atoms with Plasma Species - We consider in a qualitative manner whether a significant and temperature-dependent charge generation rate is likely to arise via the interaction of diffusing plasma species with the cesium atoms adsorbed on the walls of the Ar-Cs cavity, for the conditions indicated previously in Figs. 9 and 10. The species of interest are electrons, photons, and various ionic, metastable and excited states of argon and cesium.

The most important ion and electron loss for this very collision-dominated plasma ($n_e \approx n_+ \approx 10^{12} \text{ cm}^{-3}$, $N_0 \approx 3 \times 10^{18} \text{ atoms cm}^{-3}$) is volume recombination. The atomic Ar^+ ion is rapidly converted into the molecular Ar_2^+ ion which promptly decays via dissociative recombination with an electron. There are two dominating avenues of recombination for the atomic Cs^+ ion: at low Cs/Ar values, the Cs^+ ion is lost by collisional-radiative recombination with 2 electrons; at high Cs/Ar values, Cs^+ is converted into the molecular Cs_2^+ ion (via a Cs^+ -Cs-Ar collision) which disappears by dissociative recombination. We can therefore consider the dominant electron and ion loss paths to be via the products of recombination, viz., photons, metastable states and excited states.

Only a small fraction of the metastable states will diffuse out from the plasma to the cavity walls. For example, at gas pressures ≈ 100 torr the principal loss of argon metastable states at the lower Cs/Ar values is by 2 and 3-body collisions with neutral argon atoms which result in the production of high-energy (~ 11.5 eV) resonance and non-resonance photons. As the value of Cs/Ar increases, an increased fraction of the argon metastables are destroyed in collisions with cesium atoms yielding Cs^+ ions by the Penning process, but as indicated in the previous paragraph, the eventual outcome of such an ion generation is likely to be the production of lower excitation energy (< 3.9 eV). Thus in either case the metastable states are almost wholly destroyed in the volume of the plasma and few reach the walls.

The tentative arguments presented here suggest to us that if an important charge production process exists at the relatively cold surface of the cavity, it probably arises because of the interaction of the surface cesium atoms with the copious flux of photons from the plasma. Now since the fission fragments in their passage through the gas generate 2 argon ions for each argon metastable state (these two species being responsible for almost all the measured eV/ion pair), the decay of these species by various routes to produce photons is not expected to yield a total photon production rate very different from the volume ion generation rate. Also if we assume a very large photoelectric yield⁽¹⁰⁾ from the cesium-covered surface of 0.1 electrons/photon, then the electron production rate at the surface is ~ 0.1 of the total ion generation rate in the volume and therefore immediately too small to explain the large discrepancies between the measured and computed values of electron density as shown in Fig. 10. In addition, the back-diffusion of electrons into the surface would further greatly reduce the above production rate.

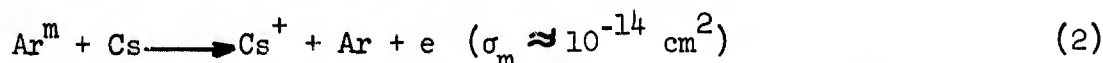
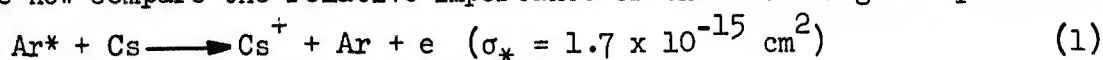
There is another reason for concluding that an electron source at the walls of the cavity will not significantly alter the spatially averaged electron density in the plasma. The injection of only electrons at the plasma boundaries will have the effect of reducing the ion-accelerating (for plasma positive ions) space-charge potential, thereby reducing the ion loss rate by ambipolar diffusion. However, since the dominant ion loss in the present case is not by diffusion but is via volume recombination, the effect of changes in the ion diffusion rate will be small.

Finally we note from Taylor and Langmuir's work on the cesium coverage of tungsten,⁽⁸⁾ that over the temperature range of interest to us, viz., 400-700°K where n_e is critically dependent on the cavity temperature, the fraction θ_n of a tungsten surface covered with cesium was insensitive to temperature for a cesium arrival rate $\mu_a \sim 10^{18}$ atoms $\text{cm}^{-2} \text{sec}^{-1}$ (as in the present experiment). Thus if Kovar behaves in a manner similar to tungsten and the adsorbed cesium layer is insensitive to temperature, photoelectric action at the surface (even if considerably underestimated in our previous arguments) would be unable to explain the observed marked dependence of electron density upon temperature.

(g) Ionization of Cesium by Argon Excited States - The equations which we use for computing the electron density in the Ar-Cs plasma do not take into account any possible ionization of cesium by argon excited states which are not metastable. The following arguments support the view that ionizing collisions of argon radiating states with cesium can be neglected in comparison with the cesium ion production rate from argon metastable states.

Most of the electrons which become excited in argon eventually fall to the ground state via the lowest $(3P)^5(4s)$ excited electron configuration which consists of two metastable states ($3P_2$ 11.53 eV, $3P_0$ 11.72 eV) and two radiating states ($3P_1$ 11.62 eV, $1P_1$ 11.81 eV). This result follows from the considerable imprisonment of resonance radiation and transfer of excitation which occurs in argon at the gas density 2.9×10^{18} atoms cm^{-3}) of the present experiment. Thus we need only consider here the influence of the $3P_1$ and $1P_1$ radiating states which present by far the greatest concentration of argon radiating states.

We now compare the relative importance of the following two processes:



where we do not distinguish between the two lowest radiating states (Ar^*) or between the two metastable states (Ar^m) because their respective energy differences are small. The ionization cross section σ_* for process (1) is that computed recently by Sheldon.⁽¹¹⁾ There are, however, no published data available for process (2); the value of σ_m shown is that inferred by Nolan⁽¹²⁾ from his measurements of ionization growth in an Ar-Cs mixture. We consider values of $\text{Cs}/\text{Ar} < 3 \times 10^{-4}$ where the discrepancy between theory and experiment (Fig. 10) is greatest and where we seek an additional ion generation rate in order to account for the high measured values of the electron density. Under these conditions, the destruction rate of Ar^m states in the gas by collisions with argon⁽¹³⁾ and cesium atoms yields a metastable lifetime $\tau_m = 10^{-5}$ sec. The total metastable generation rate S_m at an argon atom density of $2.9 \times 10^{18} \text{ cm}^{-3}$ is $5 \times 10^{15} \text{ cm}^{-3} \text{ sec}^{-1}$,⁽¹⁾ half of which is directly due to fission fragments and half of which arises indirectly through ionic recombination into metastable levels. Thus the metastable density is

$$n_m = S_m \tau_m = 5 \times 10^{10} \text{ cm}^{-3}.$$

We do not know the total generation rate S_* of the Ar^* excited states but an upper bound to S_* can be readily set by considering that the total energy deposited in the gas by the fission fragments produces exclusively Ar^* states of energy 11.7eV. This procedure yields $S_* < 9.5 \times 10^{15} \text{ cm}^{-3} \text{ sec}^{-1}$. The natural lifetime τ_* of the $3P_1$ and $1P_1$ states is expected to be in the range $10^{-8} - 10^{-10}$ sec and allowing two orders of magnitude increase in the lifetime because of repeated absorption and re-emission of the resonance radiation, we set $\tau_* \leq 10^{-6}$ sec. Thus

$$n_* = S_* \tau_* < 10^{10} \text{ cm}^{-3}$$

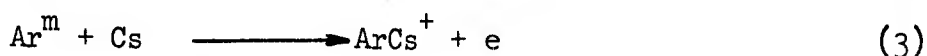
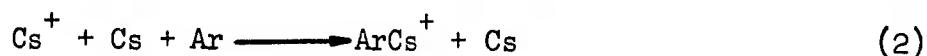
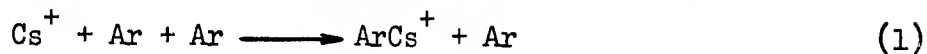
This leads to a ratio of Cs^+ production rate by excited states and metastable states of

$$\frac{n_* \sigma_*}{n_m \sigma_m} < \frac{1.7}{50} = 0.03.$$

Since this ratio is so small we conclude that the neglect of $\text{Ar}^* - \text{Cs}$ collisions in our code calculations is not the cause of the discrepancy between the theoretical and experimental values of n_e .

(h) Heteronuclear Ions - The ions which we consider as important for controlling the electron density in the Ar-Cs plasma are Ar^+ , Ar_2^+ , Cs^+ and Cs_2^+ . However, the heteronuclear ArCs^+ ion may also be present since such an ion has been isolated experimentally.⁽¹⁴⁾ Unfortunately, the influence of the ArCs^+ ion is not readily estimated because of the lack of data regarding its production and loss rates.

For our experimental conditions, it appears that the following three processes are most likely to lead to the formation of ArCs^+ :



Processes (1) and (2) are postulated on the basis of exactly analogous reactions proposed by Oskam⁽¹⁵⁾ for the conversion of Ne^+ to HeNe^+ in helium admixed with traces of neon. Process (3) has been given by Herman and Cermak⁽¹⁴⁾ and is based on their measured values of the appearance potential of ArCs^+ .

In Oskam's microwave studies of helium admixed with traces of argon, krypton and xenon, and neon admixed with traces of argon and krypton, at total pressures 5 to 25 torr, the only heteronuclear ion considered to influence the plasma electron density was HeNe^+ , i.e., the experimental results of the remaining gas mixtures could be adequately accounted for by the presence of the more usual homonuclear (Ne_2^+ , Ar_2^+ , etc.) molecular ions. However, the existence of heteronuclear noble gas ions such as HeNe^+ , HeKr^+ and NeAr^+ (in addition to noble-gas alkali metal ions such as ArCs^+) has been confirmed by mass spectroscopic studies⁽¹⁶⁾ but these studies have been conducted at gas pressures $\lesssim 4 \times 10^{-3}$ torr. Thus the stability of most of the heteronuclear ions in the collisional environment of a high pressure (100 torr) plasma is not known.

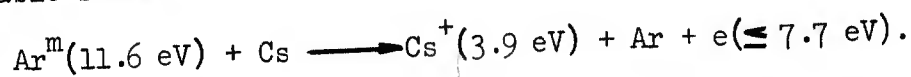
We note from the above that the low-pressure existence of NeAr^+ and the absence of any significant role by NeAr^+ in Oskam's studies at much higher pressure suggest that NeAr^+ is unstable in a collisional environment. This conclusion is supported by our own computations of electron density in the Ne-Ar system, based on Ne^+ , Ne_2^+ , Ar^+ and Ar_2^+ ions only, where good agreement is obtained with the measured values of electron density (Fig. 8). Since no information is available on the stability of ArCs^+ in the Ar-Cs plasma, there is the possibility that the critical observed dependence of n_e upon gas temperature (Fig. 10) could arise because ArCs^+ is stable at low temperatures, but dissociates at the higher temperatures.

However, it should be noted that the present computed values of n_e at the lower Cs/Ar values and temperatures of 400 to 500°K (Fig. 10) are much less than the measured values, and if ArCs^+ is introduced into the existing computations via processes (1), (2), or (3), the result is a depletion both directly and indirectly of the dominant Cs^+ ion (process (3) is presently assumed to yield the Cs^+ ion only) in exchange for the molecular ArCs^+ which would surely decay rapidly by dissociative recombination with an electron. Thus, in this case, the ArCs^+ would act as a sink to depress the calculated electron density below its already low value. On the other hand, at the high Cs/Ar value of 10^{-3} (Fig. 10) a depression of the computed curve is required to bring theory into better agreement with experiment, which tends to support the presence of an ArCs^+ ion. Also an association-dissociation reaction of the type leading to a very temperature dependent molecular ion

formation rate might reasonably be considered the cause of the sensitive dependence of n_e upon temperature.

Nevertheless, the presence of a temperature dependent ArCs^+ ion will not alone account for the results since an additional correction to the existing theory would be required at low values of Cs/Ar to bring the computed values into closer agreement with experiment.

(i) Influence of Energetic Electrons from Penning Ionization Process - The atomic Cs^+ ions are generated by collisions of atomic Cs with argon (Ar^m) metastable states:



Thus the ejected electron can possess energy ϵ up to a maximum of about 7.7 eV, i.e., the difference between the excitation energy of the argon metastable state and the ionization energy of atomic cesium. We have used a large cross section of 10^{-14} cm^2 for the above Penning process⁽¹²⁾ and have neglected the additional ionization of atomic cesium that can possibly arise from the 7.7 eV electrons during their time to reach thermal energies. We now consider the relaxation time of these hot electrons.

For electron densities $n_e = 10^{12} \text{ cm}^{-3}$, the electron relaxation time τ_r due to electron-electron and electron-ion collisions is approximately^(17,18)

$$\tau_r = \frac{0.7(T)^{3/2}}{2.63 n_e \ln \Lambda}$$

where T is the electron temperature in $^\circ\text{K}$ and Λ is a factor due to Spitzer⁽¹⁹⁾ which is the ratio of the Debye shielding distance over an average critical impact parameter. The quantity Λ is in fact just nine times the number of electrons in a Debye sphere⁽¹⁷⁾ and is given by

$$\Lambda = \frac{(12 \pi) \left(\frac{k T}{4 \pi n_e e^2} \right)^{3/2}}{n_e^{1/2}}$$

For values of $T=800^\circ\text{K}$ and $n_e = 10^{12} \text{ cm}^{-3}$, $\ln \Lambda = 3.3$. This yields a value for τ_r of 1.8×10^{-9} sec and thus we note that because of the strong influence of coulomb forces, the hot electrons are rapidly thermalized with the background electrons. The effect of hot electron - atom collisions will be to decrease

τ_r still further by a small amount — the decrease being small because only elastic collisions are permissible with argon for $\epsilon < 11.5$ eV.

We estimate, very approximately, the number f_i of Cs atoms ionized by a hot electron by using

$$f_i = n_{Cs} \sigma_i v_e \tau_r$$

where n_{Cs} is the density of Cs atoms, σ_i is some average ionization cross section for e-Cs collisions where the electron energy degrades from ~ 7 eV to below the ionization potential of cesium in times $\sim \tau_r$, and v_e is taken to be the velocity of a 5 eV electron. For a value of $Cs/Ar = 10^{-4}$, $n_{Cs} = 2.9 \times 10^{14} \text{ cm}^{-3}$ and we assume a value for σ_i of 10^{-15} cm^2 . Thus with $v_e = 1.3 \times 10^8 \text{ cm sec}^{-1}$ and $\tau_r = 1.8 \times 10^{-9} \text{ sec}$, we obtain $f_i = 0.07$.

On the basis of this result, we have therefore tentatively concluded that there exists no unusually high tail to the Maxwellian distribution of the plasma electrons and that no large error is made by neglecting the energetic electrons from the Penning process, particularly for values of $Cs/Ar \lesssim 10^{-4}$.

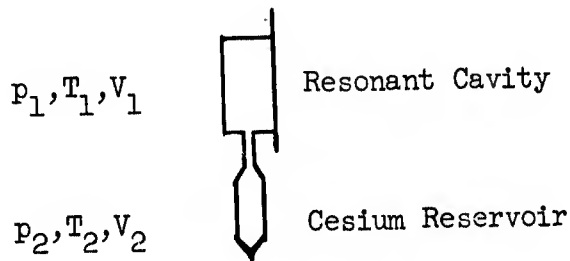
APPENDIX A

COMPUTATION OF CS/AR FOR MICROWAVE CAVITY

For the argon pressures of interest in these studies the mean free path of an atom is much less than the dimensions of the cavity so we use the ideal gas law $p=nkT$. At the conditions of seal-off the gas pressure is p_0 and the temperature is T_0 ($\sim 300^\circ\text{K}$). Therefore we have

$$p_0(\text{Ar}) = n_0(\text{Ar})kT_0. \quad (\text{A-1})$$

At operating conditions, the cavity of volume V_1 is at a temperature T_1 ($\langle T_{\text{gas}} \rangle_{\text{av}}$) and the cesium reservoir of volume V_2 is at a temperature T_2 .



From the conservation of the total number of argon atoms and assuming zero thermal expansion of the volumes

$$n_1(\text{Ar})V_1 + n_2(\text{Ar})V_2 = n_0(\text{Ar})(V_1 + V_2) = \frac{p_0}{kT_0} (V_1 + V_2) \quad (\text{A-2})$$

Now $p_1(\text{Ar})=p_2(\text{Ar})$ so from the ideal gas law

$$n_2(\text{Ar}) = \frac{T_1}{T_2} n_1(\text{Ar}) \quad (\text{A-3})$$

Substituting A-3 into A-2 gives the number density of argon in volume 1

$$n_1(\text{Ar}) = \frac{p_0}{kT_0} \frac{V_1 + V_2}{V_1 + \frac{T_1}{T_2} V_2} \quad (\text{A-4})$$

At steady state the vapor pressure of cesium in V_1 is the same as that in V_2 and is fixed by the temperature (T_2) of the liquid cesium in T_2 .

$$p_1(\text{Cs}) = p_2(\text{Cs}) = f(T_2). \quad (\text{A-5})$$

Also from the ideal gas law

$$p_1(\text{Cs}) = n_1(\text{Cs})kT_1 \quad (\text{A-6})$$

Solving A-6 for $n_1(\text{Cs})$ and dividing by $n_1(\text{Ar})$ from (A-4) gives the cesium-to-argon ratio in V_1

$$\frac{\text{Cs}}{\text{Ar}} = \frac{n_1(\text{Cs})}{n_1(\text{Ar})} = \left(\frac{p_1(\text{Cs})}{p_o} \right) \left(\frac{T_o}{T_1} \right) \left[\frac{V_1}{V_1 + V_2} + \frac{T_1}{T_2} \frac{V_2}{V_1 + V_2} \right] \quad (\text{A-7})$$

For the argon-cesium cavity $V_1=3.39 \text{ cm}^3$, $V_2=1.81 \text{ cm}^3$ and the volume fractions are therefore $V_1/(V_1+V_2)=0.65$ and $V_2/(V_1+V_2)=0.35$. For $T_o=300^\circ\text{K}$ Eq.(A-7) becomes

$$\frac{\text{Cs}}{\text{Ar}} = \left(\frac{p(\text{Cs})}{p_o} \right) \left[\frac{195}{\langle T_{\text{gas}} \rangle_{\text{av}}} + \frac{105}{T_{\text{Cs}}} \right]. \quad (\text{A-8})$$

APPENDIX B

DIFFUSION OF CESIUM IN ARGON

In the operation of the argon-cesium microwave cavity, the time to reach equilibrium (i.e. steady-state) conditions depends primarily upon the diffusion rate of cesium (in argon) between the cavity and the cesium reservoir. A change of vapor pressure of cesium in the reservoir leads to a flow of cesium between the reservoir and cavity to establish not only a new equilibrium concentration in the gas in the cavity but also a new equilibrium surface coverage on the walls of the cavity. In the following a diffusion rate is computed for an assumed non-equilibrium condition and then a time to reach equilibrium is computed for a case which starts considerably removed from equilibrium.

The equation for diffusion along a tube has been derived previously⁽¹⁾ and is

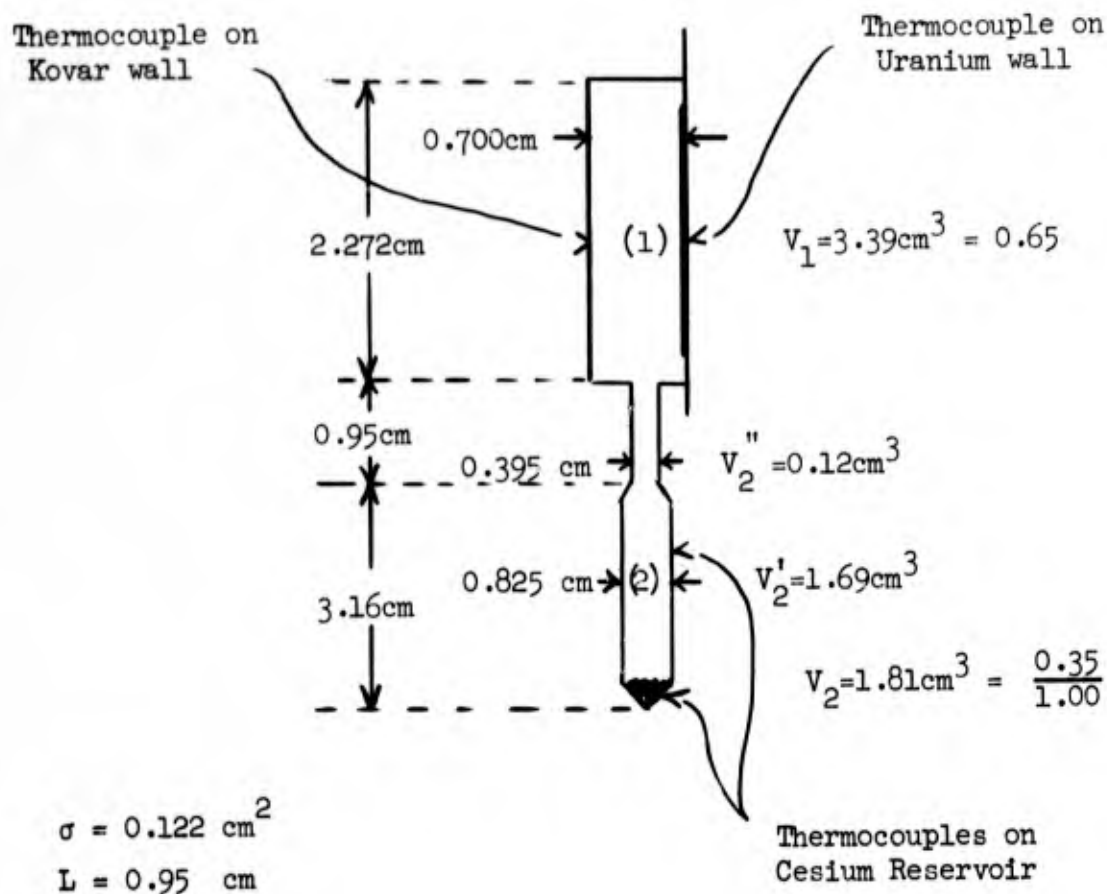
$$I_{Cs} = - \frac{1}{3} \frac{\bar{u} \sigma}{n_{Ar} Q_d} \frac{dn_{Cs}}{dz} \quad (B-1)$$

where I_{Cs} is the diffusion current passing through the cross sectional area σ of the tube, \bar{u} is the average relative velocity for collisions of argon and cesium atoms, Q_d is the momentum loss cross section, n_{Ar} is the concentration of argon atoms and dn_{Cs}/dz is the gradient of the concentration of cesium atoms (n_{Cs}) along the axis of the tube (z).

\bar{u} and n_{Ar} are actually functions of z but for this computation we assume them independent of z and also approximate the gradient as

$$\frac{dn_{Cs}}{dz} \approx - \left[\frac{n_2(Cs) - n_1(Cs)}{L} \right] \quad (B-2)$$

where $n_2(Cs)$ is the cesium density in the reservoir, $n_1(Cs)$ is the cesium density in the cavity and L is the length of the tube joining the reservoir to the cavity. The pertinent dimensions of the device are given in Fig. B-1.



Total interior cavity area:

$$S_1 = 2 \left[\frac{\pi}{4} \times (2.272)^2 \right] + \left[\pi \times 2.272 \times 0.7 \right] = 8.10 + 5.0 = 13.10 \text{ cm}^2$$

Fig. B-1. Dimensions of Ar-Cs microwave cavity.

We select as typical the following temperatures: $T(\text{ur}) = 420^\circ\text{C}$, $T(\text{k}) = 300^\circ\text{C}$ and $T(\text{Cs}) = 146^\circ\text{C}$ and therefore $\langle T_{\text{gas}} \rangle_{\text{av}} = (420 + 300)/2 = 360^\circ\text{C} = 633^\circ\text{K}$ and the average gas temperature in the connecting tube is $\langle T \rangle = (360 + 146)/2 = 253^\circ\text{C} = 526^\circ\text{K}$.

The average relative velocity is ⁽¹⁾

$$\bar{u} = \left[\frac{8k\langle T \rangle(m_{\text{Ar}} + m_{\text{Cs}})}{\pi m_{\text{Ar}} m_{\text{Cs}}} \right]^{1/2} \quad (\text{B-3})$$

and substituting $\langle T \rangle = 526^\circ\text{K}$ and the masses of argon (m_{Ar}) and cesium (m_{Cs}) we obtain $\bar{u} = 5.98 \times 10^4 \text{ cm sec}^{-1}$. The maximum diffusion current occurs when $n_1(\text{Cs}) = 0$ that is, immediately after the reservoir is brought to temperature and before any cesium has reached the cavity. At $T_2(\text{Cs}) = 146^\circ\text{C} = 419^\circ\text{K}$, $p_2(\text{Cs}) = 7.0 \times 10^{-3} \text{ torr}$ and $n_2(\text{Cs}) = p_2(\text{Cs}) / kT_2(\text{Cs}) = 1.61 \times 10^{14} \text{ cm}^{-3}$. Substituting these values and $Q_d = 5.72 \times 10^{-14} \text{ cm}^2(1)$ into Eqs. (B-3) and (B-1) we obtain for the maximum diffusion current $I_{\text{Cs}}(\text{max}) = 2.48 \times 10^{12} \text{ atoms sec}^{-1} = 8.95 \times 10^{15} \text{ atoms hr}^{-1}$.

When the partial pressure of cesium in the cavity equals that in the reservoir the total number of cesium atoms in the cavity is $N_1(\text{Cs}) = n_1(\text{Cs})V_1 = n_2(\text{Cs})V_1T_2/T_1 = 1.61 \times 10^{14} \times 3.39 \times 419 / 526 = 4.34 \times 10^{14}$ atoms of cesium. At the maximum rate the time to saturate the gas would only be $t = N_1(\text{Cs}) / I_{\text{Cs}}(\text{max}) = 0.0484 \text{ hr}$ but, of course, the driving force tends to zero as $p_1(\text{Cs}) \longrightarrow p_2(\text{Cs})$. The diffusion rate decreases as equilibrium is approached but the adsorbed layer of cesium on the inside surfaces of the cavity walls must also come to equilibrium with the partial pressure of cesium in the gas.

For a cesium atom diameter of $5.34 \times 10^{-8} \text{ cm}$, the projected area ($\pi/4 D^2$) is $2.2 \times 10^{-15} \text{ cm}^2$ per atom. From the inverse of this area, the atoms in one monolayer of adsorbed cesium is $4.5 \times 10^{14} \text{ atoms cm}^{-2}$. The cesium arrival rate at the wall surfaces $\approx n_1(\text{Cs}) \times v(\text{Cs}) \approx 10^{14} \text{ cm}^{-3} \times 10^4 \text{ cm sec}^{-1} = 10^{18} \text{ atoms cm}^{-2} \text{ sec}^{-1}$. At this arrival rate and temperature (526°K) the fraction of the surface covered (assuming surface behaves like tungsten) is ~ 0.9 .⁽⁸⁾ The inside surface area of the cavity is 13.10 cm^2 so the total number of atoms adsorbed for 0.9 of a monolayer is $N_s(\text{Cs}) = 0.9 \times 4.5 \times 10^{14} \times 13.1 = 5.3 \times 10^{15}$ atoms which is about 10 times the atoms contained in the gas ($N_1(\text{Cs}) = 4.34 \times 10^{14}$ atoms).

Overall Rate Equation

An approximate overall rate equation can be derived as follows. From Eqs. (B-1) and (B-2) the diffusion current through the throat can be written

$$I_{\text{Cs}} = k [n_2(\text{Cs}) - n_1(\text{Cs})] \quad (\text{B-4})$$

where

$$k = \frac{1}{3} \frac{\bar{u} \sigma}{n_{(\text{Ar})} Q_d L} \quad (\text{B-5})$$

The cesium diffusing through the throat builds up the concentration in the gas in the cavity and also deposits on the walls; thus

$$I_{Cs} = \frac{dn_1(Cs)}{dt} V_1 + \frac{dn_s(Cs)}{dt} S_1. \quad (B-6)$$

We assume the cesium transport rate across the cavity to the walls is large compared to the transport rate through the throat and the cesium deposition rate on the surface is proportional to the cesium concentration in the gas $n_1(Cs)$. Therefore we set

$$\frac{dn_s(Cs)}{dt} S_1 = k_2 \frac{dn_1(Cs)}{dt} V_1 \quad (B-7)$$

and combining Eqs. (B-4), (B-6) and B-7)

$$\frac{dn_1(Cs)}{dt} = \frac{1}{\tau} [n_2(Cs) - n_1(Cs)] \quad (B-8)$$

where

$$\tau = \frac{3(1 + k_2) n_{(Ar)} Q_d L V}{\bar{u} \sigma}. \quad (B-9)$$

Integrating Eq.(B-8) with $n_2(Cs)$ independent of time

$$\frac{n_1(Cs)}{n_2(Cs)} = 1 - e^{-t/\tau} \quad (B-10)$$

In this model the gas and surface coverage approach their equilibrium values together with k_2 atoms to the surface for each atom to the gas. τ is the e-folding time as equilibrium is approached.

Setting $k_2 = 10$ cesium atoms on the surface per cesium atom in the gas and substituting into Eq.(B-9) we obtain

$$\tau = \frac{3 \times 11 \times (2.9 \times 10^{18}) \times (5.72 \times 10^{-14}) \times (0.95) \times (3.39)}{(5.98 \times 10^4) \times (0.122)}$$

$$\tau = 2420 \text{ sec} = 0.675 \text{ hr.}$$

Starting with no cesium in the reservoir 90% of the equilibrium concentration should be reached after $\sim 1-1/2$ hr. After equilibrium has once been obtained and conditions are changed for a new run, the new state of equilibrium should be reached within one hour.

REFERENCES

1. C. B. Leffert, D. B. Rees, and F. E. Gifford, ONR Annual Report No. 6, Contract Nonr-3109(00), (Oct. 1965).
2. C. B. Leffert, D. B. Rees, and F. E. Jamerson, J. Appl. Phys. 37, 133 (1966).
3. D. B. Rees, C. B. Leffert, and F. E. Jamerson, Proc. IEEE Thermionic Specialist Conference (San Diego), p.166, (Oct. 1965).
4. C. B. Leffert, D. B. Rees, and F. E. Jamerson, Phys. Letters, 22, 423, (1966).
5. D. J. Rose and S. C. Brown, J. Appl. Phys. 23, 1027 (1952).
6. M. A. Heald and C. B. Wharton, Plasma Diagnostics with Microwaves, (Wiley) (1965).
7. M. Kaminsky, "Atomic and Ionic Impact Phenomena on Metal Surfaces", Academic Press (1965) p.99.
8. J. B. Taylor and I. Langmuir, Phys. Rev. 44, 423 (1933).
9. Solid State Physics, Advances in Research and Applications, Vol. 2, Ed: F. Seitz and D. Turnbull, Academic Press, (1956) p.355.
10. G. L. Weissler, Handbuch der Physik, Ed. S. Flugge, (Springer-Verlag), vol. XXI, 304 (1956). Photoelectric yields are given for pure and compound surfaces in all cases ≤ 0.1 electrons/quantum.
11. J. W. Sheldon, J. Appl. Phys., 37, 2928 (1966).
12. J. F. Nolan, Private communication (1964).
13. A. V. Phelps and J. P. Molnar, Phys. Rev., 89, 1202 (1953); A. H. Futch and F. A. Grant, Phys. Rev., 104, 356 (1956).
14. Z. Herman and V. Cermak, Nature, 199, 588 (1963).
15. H. J. Oskam, Philips Res. Repts., 13, 335 (1958).
16. M.S.B. Munson, J. L. Franklin and F. H. Field, J. Chem. Phys., 67, 1542 (1963).
17. D. J. Rose and M. Clark, Jr., Plasmas and Controlled Fusion, (MIT and Wiley) (1961), p.165.
18. J. L. Delcroix, Introduction to the Theory of Ionized Gases, (Interscience) (1960), p. 112.
19. L. Spitzer, Jr., Physics of Fully Ionized Gases, (Interscience) (1956), p.78.

SECTION B

CONTENTS

ABSTRACT	1
I. OBJECT	1
II. CONCLUSIONS	1
III. INTRODUCTION	2
IV. ANALYTIC SOLUTION TO TRANSPORT EQUATIONS FOR A DIFFUSION CONTROLLED PLASMA	3
Transport Equations for a Collision-Dominated Plasma .	3
Boundary Conditions - Sheath Equations	4
Analytic Solutions	6
Volume Recombination Limit to Applicability of Diffusion Model	6
V. COMPUTER PROGRAM	8
VI. PARAMETER STUDIES	8
I-V Characteristic for Trial Problem	8
Effect of Richardson Current (J_R)	11
Effect of Ion Generation Rate (S)	11
Effect of Electrode Spacing (d)	11
VII. REFERENCES	14
APPENDIX A - PROBLEM STATEMENT	15
APPENDIX B - PROGRAM LISTING AND SAMPLE OUTPUT	22

SECTION B

ELECTRON TRANSPORT IN A DIFFUSION CONTROLLED PLASMA: DESCRIPTION OF COMPUTER PROGRAM AND PARAMETRIC STUDIES

ABSTRACT

The computer program is described for the diffusion model of the electron transport problem in which the plasma is generated by fission fragments and decays by ambipolar diffusion to the electrodes. In the temperature range of thermionic energy conversion the upper limit of applicability of this model, where volume charge loss becomes appreciable, is shown to be at an electron density of $\sim 2 \times 10^{12} \text{ cm}^{-3}$. Parametric studies on the Richardson current, ion generation rate and electrode spacing showed that for diode currents of interest in a practical energy converter ($1 \leq J \sim 10 \text{ amps cm}^{-2}$) the necessary electron density was beyond the limit of applicability of this theory.

I. OBJECT

To program the equations of the analytic solution of the diffusion model of the electron transport problem for computation on the IBM 7094 computer and to perform sufficient computations to ascertain the applicability of this model to our noble gas thermionic energy converter studies.

II. CONCLUSIONS

1. The basic hypothesis for this model of charge loss by ambipolar diffusion is applicable for low electron densities and small spacings (e.g. $n_e < 2 \times 10^{12} \text{ cm}^{-3}$ for $d=0.1 \text{ cm}$) where volume recombination losses are negligible.
2. For diode currents of interest in practical thermionic energy converters ($1 \leq J \sim 20 \text{ amps cm}^{-2}$), the predicted electron densities exceed the limit of applicability of this model and enter the range of appreciable volume charge loss.
3. A solution of the electron transport problem is needed which also includes volume loss of the charges wherein a higher electron density is available for electron transport.

4. This diffusion model with a uniform volume ionization rate from fission fragments predicts considerable variation in the electron density between the emitter and collector; typically $n_e(\text{max})/n_e(\text{min}) \sim 40$.
5. The calculated diode current was very sensitive to the ion generation rate and diode spacing is expected. For the plasma limited conditions studied, the diode current was relatively insensitive to the emitter Richardson current.

III. INTRODUCTION

The output power from a thermionic energy converter is strongly dependent on the electron transport properties of the interelectrode plasma. The conductivity of the plasma is proportional to the electron number density so that in our recent studies on noble gas plasmas generated by fission fragments⁽¹⁾ we have concentrated on maximizing the electron number density by maximizing the ion generation rate⁽²⁾ and minimizing the ion loss rate.⁽³⁾ These studies were made in the absence of thermionic electrons. With high current densities of thermionic electrons in a practical energy converter the electron density distribution across the plasma is itself influenced by the net current across the plasma. This implicit dependence of current on electron density distribution makes the voltage characteristic for a thermionic converter very difficult to compute.

In an earlier attempt⁽⁴⁾ to compute the I-V characteristic for our noble gas thermionic converter at low current densities, the transport properties of the plasma were ignored and the I-V characteristic was computed from considerations of just the random ion and electron currents at the plasma edge-sheath regions. This theory assumed a uniform electron density distribution across the plasma and the computed I-V curves agreed with the shape of the experimental curves at low currents but not in the region approaching saturation of the current density.

Recently a diffusion theory was formulated by Rees⁽³⁾ for the transport of thermionic electrons through a plasma contained by parallel plane electrodes. The current-voltage characteristic was derived for a plasma generated by fission fragments and which decays by ambipolar diffusion to the walls of the diode. Volume charge loss was not included. This report describes

the computer program which solves the analytic expressions for the current-voltage characteristic. Some parametric studies using this code are discussed.

This diffusion model is applicable to a plasma diode operating at low values of pressure and gap separation* where the electron density is moderate ($n_e < 10^{12} \text{ cm}^{-3}$). For the conditions of a practical thermionic energy converter ($n_e \approx 10^{13}$) the volume charge loss is expected to be appreciable or even to dominate in which case the diffusion model would not be applicable.

IV. ANALYTIC SOLUTION TO TRANSPORT EQUATIONS FOR A DIFFUSION CONTROLLED PLASMA

Transport Equations for a Collision-Dominated Plasma

The motion of positive ions (of various species, i) and electrons at a point in a gas may be expressed in terms of the concentration gradients and electric field at that point (in which they are at equilibrium) as:

$$\Gamma^- = n^- \bar{v}^- = -D^- \nabla n^- - \mu^- E n^- \quad (1)$$

$$\Gamma_i^+ = n_i^+ \bar{v}_i^+ = -D_i^+ \nabla n_i^+ + \mu_i^+ E n_i^+ \quad (2)$$

$$\Gamma_{\text{net}} = \Gamma^- - \sum_i \Gamma_i^+ \quad (3)$$

where Γ represents particle current density; n is particle density; \bar{v} is the average drift velocity; D , the diffusion coefficient; μ , the mobility; E , the electric field; and Γ_{net} is the total resultant current. Considerable simplification is obtained with the assumptions of:

- (1) a predominant (or an effective) ion species, $n^+ = \sum_{i=1}^l n_i^+ / l$;
- (2) a quasi-neutral plasma, $(n^+ - n^-) \ll n^-$ so $n^+ \approx n^- = n$,
(Consequently, from Poisson's equation $dE/dx = (e/\epsilon_0)(n^- - \sum_i n_i^+) \approx 0$);
- (3) diffusion and mobility coefficients which are independent of the temperature variations across the interelectrode gap but which do vary with the average temperature of the respective particles; and

*The limitation of this theory to small gap spacing means that these results do not apply to the microwave cavities used in the experiments of Section A.

(4) parallel plane geometry ($\nabla \rightarrow d/dx$) where $\lambda_D < \lambda_e \ll d$ and λ_D is the Debye length for electrons, λ_e is the electron-neutral atom mean free path and d is the interelectrode spacing.

With these assumptions the particle transport equations simplify to

$$\frac{dn}{dx} = - \frac{1}{D_a} \left[\Gamma^- - \left(\frac{\mu^-}{\mu^+ + \mu^-} \right) \Gamma_{\text{net}} \right] \quad (4)$$

where $D_a = (D^+ \mu^- + D^- \mu^+) / (\mu^+ + \mu^-)$ is the ambipolar diffusion coefficient.

When volume charge loss is included, the continuity equations for the charges can be expressed in terms of the ion generation rate ($S(\vec{r})$) and an effective volume recombination coefficient $\alpha'(N_0, n)$ as

$$\frac{d\Gamma^-}{dx} = \frac{d\Gamma^+}{dx} = S(x) - \alpha'(n) (n(x))^2 \quad (5)$$

The analytic solution to Eqs. (4) and (5) is not known when the last term is not negligible. Although the model will be somewhat restrictive it was desired to obtain the analytic solution for the simpler case of diffusion loss only. Consequently with the further assumptions of

(5) negligible volume charge loss ($\alpha' n^2 \ll (D^-/\Lambda^2)n$) and

(6) uniform ion generation rate, $S = \bar{S} = \int_V S(\vec{r}) d\vec{r} / V$,

equation (5) reduces to

$$\frac{d\Gamma^-}{dx} = \frac{d\Gamma^+}{dx} = S. \quad (6)$$

Substituting Γ^- from (6) into (4) and integrating gives the expression for the plasma density across the plasma⁽³⁾

$$n(x) = n(x=0) - \left(\frac{S}{2D_a} \right) x^2 - \frac{x}{D_a} \left[K_2 + \left(\frac{\mu^+}{\mu^- + \mu^+} \right) \Gamma_{\text{net}} \right] \quad (7)$$

where $K_2 = \Gamma^+ - Sx$.

Boundary Conditions - Sheath Equations

In an operating thermionic converter, the plasma is bounded by sheaths at the electrode surfaces which are negligible in thickness (unignited mode) compared to the distance between the electrodes. The potential diagram in Fig. 1 shows the thickness of the sheaths greatly exaggerated. The electron

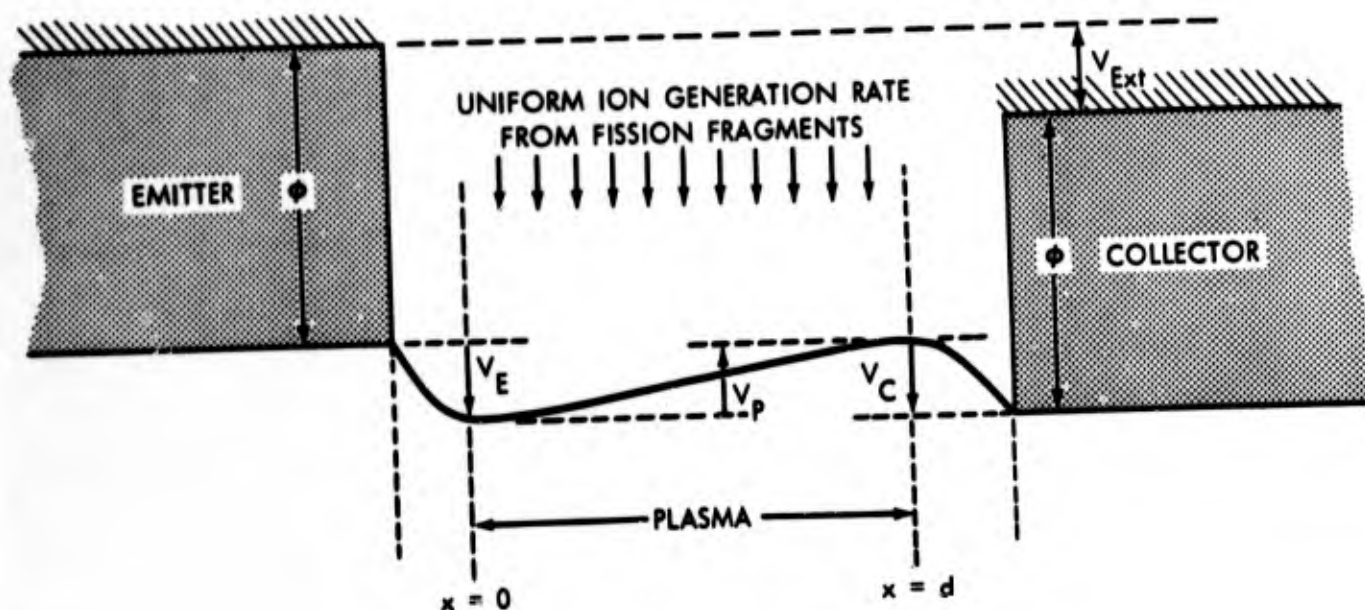


Fig. 1. Schematic of potential distribution across diode.

and ion currents to and from the plasma across the sheaths provide the boundary conditions to complete the solution of Eq.(7) for $n(x)$ and Eq.(1) for E . For a given net current ($\Gamma_{\text{net}} = J_{\text{net}}(\text{A/cm}^2)/e$) the voltage drop across the plasma ($V_P = -\int_0^d E dx$) can be computed and combined with the sheath potentials and electrode work functions to give the voltage drop across the diode. The assumptions made here are

- (7) collisionless sheaths;
- (8) Maxwellian distribution of ion and electron velocities in the plasma where,
- (9) the ion temperature (T^+) and electron temperature (T^-) of the plasma at the edges near the sheaths are set equal to the corresponding electrode temperature (T_E or T_C) and
- (10) the ion, electron, and gas temperatures in the main bulk of the plasma are set equal to the mean electrode temperature ($T_P = (T_E + T_C)/2$);
- (11) the thermionic Richardson current from the emitter is always sufficiently greater than the random current from the plasma at the emitter that the emitter sheath is electron-rich and the emitter sheath potential always retarding to ion flow from the plasma; and

- (12) the thermionic Richardson current from the collector is negligible and the collector sheath potential will depend upon the magnitude of the net current. (This requires formulations of the collector sheath equations both for ion-retarding to the plasma and also electron-retarding to the plasma.)

Analytic Solutions

The analytic solutions for both the ion-rich and electron-rich collector sheaths have been presented elsewhere.⁽³⁾ These equations, however, were not in a form that could be programmed directly for solution on the computer. The equations were reformulated and are presented in the Problem Statement in Appendix A.

The measurable potential difference between the electrodes of a thermionic converter is given in terms of the difference in work functions of the emitter (ϕ_E) and collector (ϕ_C) and the internal diode voltage (V) as

$$\text{Diode Voltage} = (\phi_C - \phi_E) + V$$

The electrode work functions are independent of the plasma and sheath potentials so we set $\phi_C = \phi_E$ and calculate I versus V . The resulting I - V characteristic can readily be corrected for a work function difference by shifting the curve along the V -axis by $(\phi_C - \phi_E)$.

Volume Recombination Limit and Applicability of Diffusion Model

When the volume recombination loss of ions is included in Eq.(5) the analytic solution to Eqs.(4) and (5) cannot be found. Nevertheless the error introduced by neglecting this term can be estimated from the diffusion solution for the case where the error is small and the solution would be only slightly perturbed. If we set an upper limit on the error, an upper bound can be computed for the electron number density for which the diffusion model is applicable.

We arbitrarily set the limit of validity of the diffusion model in terms of the ion diffusion loss (L_D) and ion recombination loss (L_R) as $L_R/L_D < \epsilon$ where ϵ is a small fraction like 0.1. In the diffusion model L_D is equal to the ion generation rate (Sd) so we have

$$\frac{L_R}{Sd} = \frac{\int_0^d \alpha' n(x)^2 dx}{Sd} < \epsilon \quad (8)$$

Substituting $n(x)$ from Eqs.(7) and (8) gives

$$\frac{L_R}{Sd} = \frac{\alpha'}{S} \left\{ n_o^2 - \left[\frac{2}{3} C_1 d^2 + C_2 d \right] n_o + \frac{C_1^2 d^4}{5} + \frac{C_1 C_2 d^3}{2} + \frac{C_2^2 d^2}{3} \right\} \quad (9)$$

where: $C_1 = S/2 Da$ (10)

and $C_2 = \frac{1}{Da} \left[K_2 + \left(\frac{\mu^+}{\mu^+ + \mu^-} \right) \Gamma_{net} \right]$ (11)

Also, using Eq.(7), the average electron (or ion) density across the gap is

$$\bar{n} = \frac{1}{d} \int_0^d n(x) dx = n_o - \frac{C_1 d^2}{3} - \frac{C_2 d}{2} \quad (12)$$

and L_R/Sd can be expressed in terms of \bar{n} from Eqs. (8) and (12) as

$$\frac{L}{Sd} = \frac{\alpha'}{S} [\bar{n}^2 + K] < \epsilon \quad (13)$$

where

$$K = \frac{C_1^2 d^4}{30} + \frac{C_1 C_2 d^3}{3} + \frac{C_2^2 d^2}{12} \quad (14)$$

Finally the range on the average electron density (\bar{n}) where the volume recombination loss can be neglected in comparison to the diffusion loss is

$$\bar{n} < \sqrt{\frac{S\epsilon}{\alpha'} - K} \quad (15)$$

The sample problem in reference (5) was chosen for a noble gas thermionic converter operating in the reduced neutron flux of a research reactor ($\phi=1.0 \times 10^{13} \text{ cm}^{-2} \text{ sec}^{-1}$) at selected conditions which are not necessarily optimum. For this problem $S=1.1 \times 10^{16} \text{ cm}^{-3} \text{ sec}^{-1}$ and $K=4.41 \times 10^{24} \text{ cm}^{-6}$. From the reaction kinetics studies for neon-argon⁽³⁾ at these conditions $\alpha'=(S-D_a n/\Delta^2)/n^2=2.8 \times 10^{-9} \text{ cm}^3 \text{ sec}^{-1}$ which is near the minimum value. Substituting these values in (15) with $\epsilon=0.1$ we find $\bar{n} < 2 \times 10^{12} \text{ cm}^{-3}$ and conclude that this diffusion model may be useful in the analysis of the forthcoming inpile transport experiment but another model which includes volume recombination loss of the charges will be needed to predict the current-voltage characteristics for a practical converter ($n \geq 10^{13} \text{ cm}^{-3}$).

V. COMPUTER PROGRAM

This program computes the current-voltage characteristic from the analytic solution to the diffusion model of the transport equations. The equations for the analytic solution are presented in the problem statement in Appendix A and the flow of the program is essentially the reverse of the order of presentation of the equations. Selected values of the net diode current are input and the diode voltage (for $\phi_E = \phi_C$) is output. Other input variables are listed in Table A-1.

A listing of the program is given in Table B-1 of Appendix B. The code output from the trial problem is given in Table B-2 and a sample input data sheet is shown in Table B-3.

VI. PARAMETER STUDIES

After checkout of the code, parameter studies were initiated to investigate the influence on the I-V characteristic of the magnitudes of the electrode spacing (d), the ion generation rate (\bar{S}) and the Richardson current density (J_R). The results of these runs are summarized in this section. A summary of the results is presented in Table I.

I-V Characteristic for Trial Problem

The I-V characteristic for the trial problem (see reference (3) and Table A-I) for $d=0.1$ cm, $S=1.1 \times 10^{16}$ cm⁻³sec⁻¹ and $J_R=2.0$ A/cm² is shown in Fig. 2. The absolute value of the net current density is plotted on the log scale on the ordinate. The code will also calculate the voltage for negative values of the current. The curve is in agreement with the hand calculated values of reference (3). The electron density distribution across the gap is shown in the insert of Fig. 2 with $n_o=2.1 \times 10^{11}$ cm⁻³ and $n_d=0.328 \times 10^{11}$ cm⁻³. The average electron density from Eq.(12) is 0.87×10^{12} cm⁻³ which is considerably higher than the values at the plasma-sheath boundaries.

TABLE I. Summary of results from parameter studies.

Run No.	d cm	Sx10 ⁻¹⁶ cm ⁻³ sec ⁻¹	J _R A cm ⁻²	J _{sat} A cm ⁻²	at J _{net} =J _{sat}		
					n _o	n _d	<n>
(A) Effect of J _R							
10.1-11	0.1	1.1	2.0	0.0856	0.262x10 ¹²	0.115x10 ¹²	0.94x10 ¹²
19.1	0.1	1.1	4.0	0.0878	0.385	0.118	1.02
20.1	0.1	1.1	6.0	0.0894	0.480	0.120	1.06
12.1-14.1	0.1	2.2	2.0	0.1681	0.352x10 ¹²	0.225x10 ¹²	1.81x10 ¹²
21.1	0.1	2.2	4.0	0.1712	0.525	0.229	1.89
34.1	0.1	10.0	0.5	0.740	0.220x10 ¹²	0.991x10 ¹²	7.52x10 ¹²
32.1	0.1	10.0	1.0	0.742	0.376	0.995	7.68
33.1	0.1	10.0	5.0	0.756	1.12	1.01	8.02
22.1	0.1	10.0	10.0	0.766	1.69	1.03	8.29
(B) Effect of S							
10.1-11	0.1	1.1	2.0	0.0856	0.262x10 ¹²	0.115x10 ¹²	0.94x10 ¹²
12.1-14.1	0.1	2.2	2.0	0.168	0.352	0.225	1.81
15.1-17.1	0.1	3.3	2.0	0.250	0.414	0.335	2.64
18.1	0.1	4.4	2.0	0.332	0.462	0.445	3.48
25.1	0.1	4.0	10.0	0.315	1.14x10 ¹²	0.421x10 ¹²	3.52x10 ¹²
24.1	0.1	6.0	10.0	0.466	1.36	0.624	5.16
23.1	0.1	8.0	10.0	0.616	1.54	0.825	6.69
22.1	0.1	10.0	10.0	0.766	1.69	1.03	8.29
28.1	0.1	50.0	10.0	3.73	3.07	5.00	3.91x10 ¹³
29.1	0.1	100.0	10.0	7.42	3.76	9.95	7.58x10 ¹³
(C) Effect of d							
27.1	0.01	10.0	10.0	0.144	0.576x10 ¹²	0.194x10 ¹²	0.455x10 ¹²
26.1	0.05	10.0	10.0	0.403	1.25	0.539	2.65
22.1	0.10	10.0	10.0	0.766	1.69	1.03	8.29
30.1	0.50	10.0	10.0	3.76	3.07	5.04	1.93x10 ¹⁴
31.1	1.0	10.0	10.0	7.53	3.73	1.01x10 ¹³	7.04x10 ¹⁴

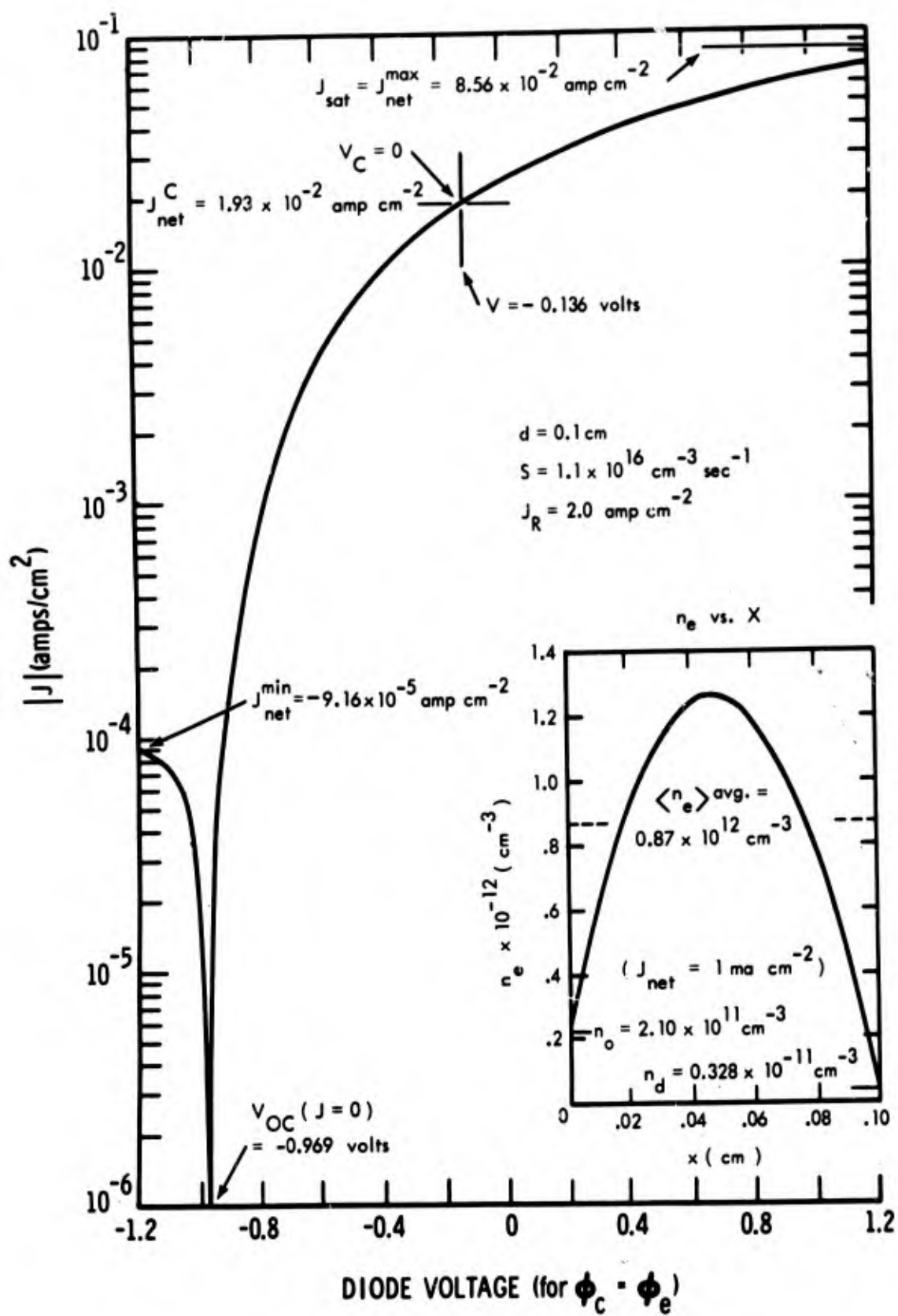


Fig. 2. I-V characteristic for trial problem.

Effect of Richardson Current (J_R)

The effect of varying just the Richardson thermionic electron current from the emitter (J_R) on the saturation current density (J_{sat}) is shown in Table I-A for a diode spacing of $d=0.1$ cm and three values of $S=1.1 \times 10^{16}$, 2.2×10^{16} and $1.0 \times 10^{17} \text{ cm}^{-3} \text{ sec}^{-1}$. The effect is very small since J_{sat} is fixed primarily by the random electron current density at the collector (providing J_R random electron current density at the collector). From Eq.(A-36) $J_{sat} = q(v_C^-)n_d^{\max} = (0.746 \times 10^{-12})n_d$. The random electron current depends strongly on the ion generation rate (S) and this is reflected in the increase of J_{sat} as S is increased from 1.1×10^{16} to $1.0 \times 10^{17} \text{ cm}^{-3} \text{ sec}^{-1}$. The electron densities at the plasma sheath interfaces are recorded in Table I as well as the average value $\langle n \rangle$ calculated from Eq.(12). $\langle n \rangle$ varies from $\sim 10^{12} \text{ cm}^{-3}$ at $S=1.1 \times 10^{16} \text{ cm}^{-3} \text{ sec}^{-1}$ to $\sim 10^{13}$ for $S=1.0 \times 10^{17} \text{ cm}^{-3} \text{ sec}^{-1}$ so that from the criterion of applicability in (15), volume recombination loss of ions would be appreciable above $S \approx 3 \times 10^{16} \text{ cm}^{-3} \text{ sec}^{-1}$.

Effect of Ion Generation Rate (S)

The effect of the ion generation rate (S) on J_{sat} and n_e is shown further in part B of Table I where S is varied from 1.1×10^{16} to $1 \times 10^{18} \text{ cm}^{-3} \text{ sec}^{-1}$.

The effect of the ion generation rate (S) on the shape of the I-V characteristic is shown in Fig. 3. To obtain $J > 1 \text{ A cm}^{-2}$ for $d=0.1$ cm would require $S \sim 10^{18} \text{ cm}^{-3} \text{ sec}^{-1}$ but as shown in Table I the electron density for these conditions greatly exceeds the limit of applicability of the diffusion model, Eq.(15).

The open circuit voltage (V at $J=0$) increases ($|V|$ decreases) as the ion generation rate increases. This is a consequence of the increased random electron current from the plasma to the emitter which lowers the emitter sheath potential drop ($|V_E|$, Eq.A-3) and this in turn lowers the diode voltage (Eq.A-1).

Effect of Electrode Spacing (d)

The effect of the electrode spacing (d) on J_{sat} and n_e is shown in Table I-C and the effect on the I-V characteristics in Fig. 4. A value of $J > 1 \text{ A cm}^{-2}$ was obtained for $d=0.5$ cm at $S=1.0 \times 10^{17} \text{ cm}^{-3} \text{ sec}^{-1}$ but again the electron density is beyond the range of applicability of the diffusion model, Eq.(15).

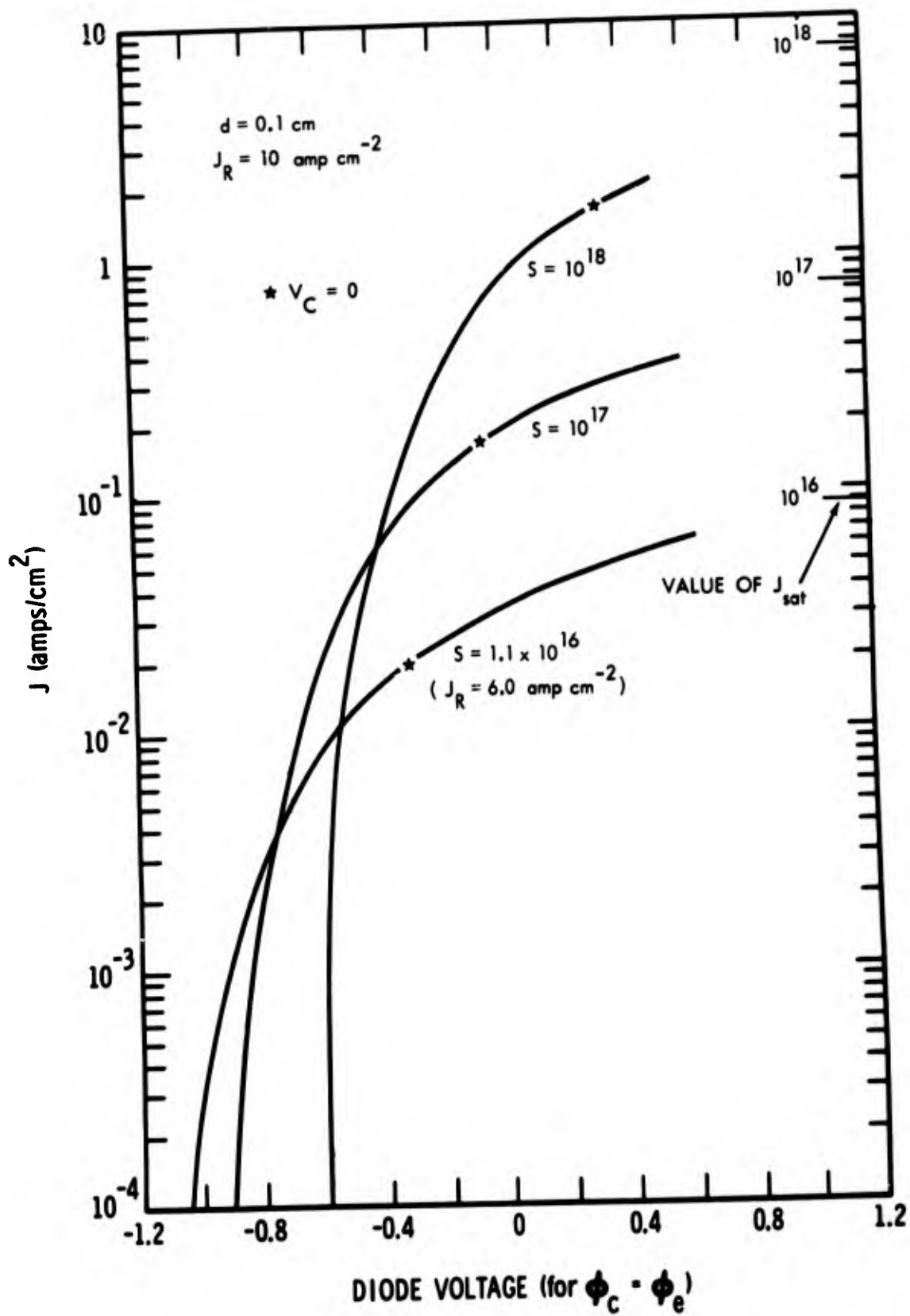


Fig. 3. I-V characteristic for various values of ion generation rate (S).

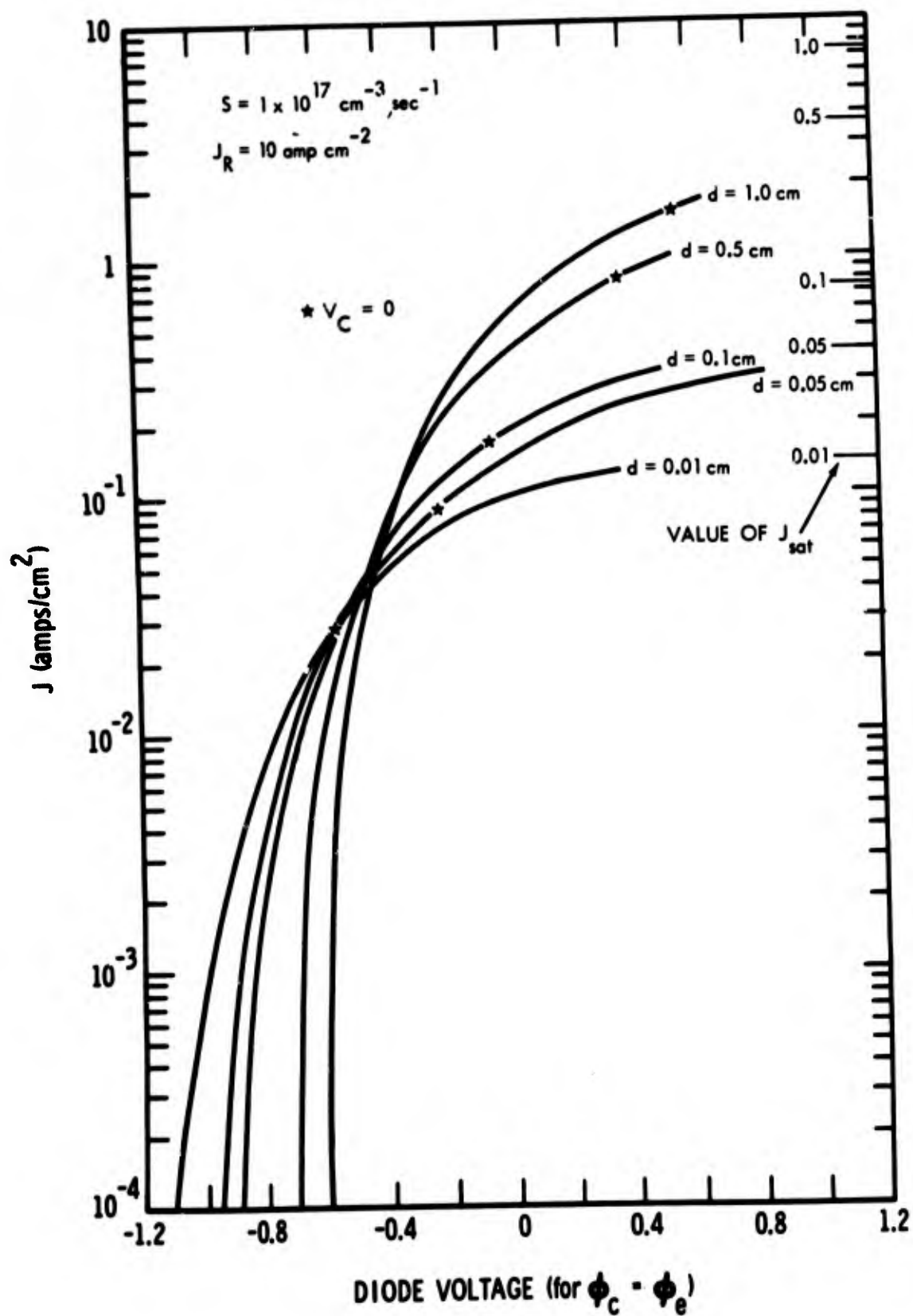


Fig. 4. I-V characteristic for various values of diode spacing (d).

VII. REFERENCES

1. C. B. Leffert, D. B. Rees, and F. E. Jamerson, J. Appl. Phys. 37, 133 (1966).
2. C. B. Leffert, D. B. Rees, and F. E. Jamerson, ONR Annual Report No. 5, Contract Nonr-3109(00) (Oct., 1964).
3. C. B. Leffert, D. B. Rees, and F. E. Gifford, ONR Annual Report No. 6, Contract Nonr-3109(00) (Oct. 1965).
4. C. B. Leffert, Adv. Energy Conv. 2, 417 (1962).

APPENDIX A - PROBLEM STATEMENT

ELECTRON TRANSPORT PROGRAM (DIFFUSION ONLY)

Internal Diode Voltage from Net Diode Current

$$(\text{Diode Voltage} = V + (\phi_C - \phi_E))$$

Solve for the internal diode voltage V , where

for $(J_{\text{net}}^{\text{min}} < J_{\text{net}} \leq J_{\text{net}}^C)$

$$V = - (V_E + V_C - V_P) \quad (\text{A-1})$$

and for $(J_{\text{net}}^C < J_{\text{net}} < J_{\text{net}}^{\text{max}})$

$$V = - (V_E - V_C - V_P) \quad (\text{A-2})$$

Symbols are defined in Table A-I and the boundary currents $J_{\text{net}}^{\text{min}}$, J_{net}^C , and $J_{\text{net}}^{\text{max}}$ will be defined last.

The emitter sheath potential V_E is given by

$$V_E = - \left(\frac{T_E}{11,600} \right) \ln \left[\frac{J_{\text{net}} + n_o v_E^-}{v_E + n_o v_E^+} \right] \text{ and} \quad (\text{A-3})$$

the collector sheath potential V_C by

for $(J_{\text{net}}^{\text{min}} < J_{\text{net}} \leq J_{\text{net}}^C)$

$$V_C = - \left(\frac{T_C}{11,600} \right) \ln \left[\frac{v_C^+ + J_{\text{net}}/n_d}{v_C^-} \right] \text{ and} \quad (\text{A-4})$$

for $(J_{\text{net}}^C < J_{\text{net}} < J_{\text{net}}^{\text{max}})$

$$V_C = - \left(\frac{T_C}{11,600} \right) \ln \left[\frac{S_d - n_o v_E^+ + \left(\frac{J_{\text{net}} + n_o v_E^-}{v_E + n_o v_E^+} \right)}{n_d v_C^+} \right]. \quad (\text{A-5})$$

The plasma potential drop V_P is given by

$$V_P = \frac{D^+}{\mu^+} \left[\ln (c + bd - d^2) - \ln(c) \right] + \left(\frac{4 D^+ \Gamma_{net}}{S (\mu^+ + \mu^-) \sqrt{b^2 + 4c}} \right) \times$$

$$\left\{ \ln \left[\frac{(\sqrt{b^2 + 4c} - b)/2 + d}{(\sqrt{b^2 + 4c} + b)/2 - d} \right] - \ln \left[\frac{(\sqrt{b^2 + 4c} - b)/2}{(\sqrt{b^2 + 4c} + b)/2} \right] \right\} \quad (A-6)$$

where:

$$b = 2A_2/A_1, \quad (A-7)$$

$$c = 2n_0/A_1, \quad (A-8)$$

$$A_1 = S/D_a \text{ and} \quad (A-9)$$

for $(J_{net}^{min} < J_{net} \leq J_{net}^C)$

$$A_2 = \frac{1}{D_a} \left[Sd - n_d v_C^+ - \left(\frac{\mu^+}{\mu^+ + \mu^-} \right) \Gamma_{net} \right] \quad (A-10)$$

and for $(J_{net}^C < J_{net} < J_{net}^{max})$

$$A_2 = \left[\frac{n_0 v_E^+ \exp \left[-\frac{\Gamma_{net} + n_0 v_E^-}{v_E^+ + n_0 v_E^+} \right]}{D_a} - \left(\frac{\mu^+}{\mu^+ + \mu^-} \right) \frac{\Gamma_{net}}{D_a} \right] \quad (A-11)$$

The electron density n_0 in the plasma near the emitter sheath and near the collector sheath (n_d) is given by

$$n_0 = \left(\frac{D}{2C} \right) \left[-1 + \sqrt{1 + 4 \left(\frac{A}{B} \right) \left(\frac{C}{B} \right)} \right] \quad (A-12)$$

and
$$n_d = \frac{n_o}{A} - \frac{B}{A} \quad \text{where} \quad (A-13)$$

for $(J_{\text{net}}^{\text{min}} < J_{\text{net}} \leq J_{\text{net}}^C)$

$$A = 1 + \frac{d v_C^+}{D_a} \quad (A-14)$$

$$B = \frac{d}{D_a} \left(\frac{\mu^+}{\mu^+ + \mu^-} \right) \Gamma_{\text{net}} - \frac{Sd^2}{2 D_a} \quad (A-15)$$

$$C = v_E^- v_E^+ + \frac{v_E^+ v_C^+}{A} \quad (A-16)$$

$$D = v_E^+ \Gamma_{\text{net}} - v_E^+ Sd - \frac{v_E^+ v_C^+ B}{A} + \frac{v_E v_C^+}{A} \quad (A-17)$$

$$E = - \frac{v_E v_C^+ B}{A} - Sd v_E \quad (A-18)$$

and for $(J_{\text{net}}^C < J_{\text{net}} < J_{\text{net}}^{\text{max}})$

$$A = 1 + \frac{d v_C^-}{D_a} \quad (A-19)$$

$$B = - \frac{d}{D_a} \left(\frac{\mu^-}{\mu^+ + \mu^-} \right) \Gamma_{\text{net}} - \frac{Sd^2}{2 D_a} \quad (A-20)$$

$$C = v_E^+ v_E^- + \frac{v_E^+ v_C^-}{A} \quad (A-21)$$

$$D = - Sd v_E^+ - \frac{v_E^+ v_C^- B}{A} + \frac{v_E v_C^-}{A} \quad (A-22)$$

$$E = - \frac{v_E v_C^- B}{A} - Sd v_E - \Gamma_{\text{net}} v_E \quad (A-23)$$

The random particle current density Γ_i^j of the charge carriers ($j = -$ for electrons, $= +$ for ions) in the plasma near the electrodes ($i = E$ for emitter, $= C$ for collector) are defined in terms of the particle density ($n=n^-=n^+$) and the average velocities $\overline{v_i^j}$ as

$$\Gamma_i^j = \frac{n \overline{v_i^j}}{4} \quad (A-24)$$

where

$$\overline{v_i^j} = \left(\frac{8 k T_i}{\pi m_j} \right)^{1/2} \quad (A-25)$$

We use the rationalized MKS system except that we prefer the number densities in units of cm^{-3} and the velocities in units of cm sec^{-1} and since the number 4 always appears with $\overline{v_i^j}$, we set

$$\Gamma_i^j, \text{ cm}^{-2} \text{ sec}^{-1} = n, \text{ cm}^{-3} \times v_i^j, \text{ cm sec}^{-1} \quad (A-26)$$

where

$$v_i^j, \text{ cm sec}^{-1} = 100 \frac{\overline{v_i^j}}{4} = \left[100 \times \left(\frac{k}{2\pi m_j} \right)^{1/2} \right] (T_i)^{1/2}. \quad (A-27)$$

This equation is used to calculate v_E^+, v_E^-, v_C^+ and v_C^- .

The mobilities of the charge carriers, μ^j , are defined in terms of the mobilities at 1 torr and 273°K , by

$$\mu^j = \frac{\mu_o^j}{p} \quad (A-28)$$

where p is the gas pressure in torr and j is defined above.

The minimum current density ($J_{\text{net}}^{\text{min}}$) is the value of the current density as the collector is driven negative with respect to the emitter. It is given by

$$J_{\text{net}}^{\text{min}} = q \Gamma_{\text{net}}^{\text{min}} = -q n_d^{\text{min}} v_C^+ = -q v_C^+ \left(\frac{n_o^{\text{min}} + \beta}{\delta} \right) \quad (A-29)$$

where $\beta = (Sd^2)/2 D_a$ (A-30)

and $\delta = 1 + \frac{d}{D_a} \left(\frac{\mu^-}{\mu^+ + \mu^-} \right) v_C^+$ (A-31)

and $n_o^{\min} = \left(\frac{B}{2A} \right) \left[-1 + \sqrt{1 - 4 \left(\frac{A}{B} \right) \left(\frac{C}{B} \right)} \right]$ (A-32)

The factors in (A-32) are given by

$$A = v_E^- v_E^+, \quad (A-33)$$

$$B = (v_E v_C^+ / \delta) - Sd v_E^+ \quad (A-34)$$

$$C = (v_E \beta v_C^+ / \delta) - Sd v_E. \quad (A-35)$$

The maximum current (J_{net}^{\max}) is the maximum value of the net current density or the saturation value of the current density as the collector is driven positive with respect to the emitter. It is given by

$$J_{\text{net}}^{\max} = q J_{\text{net}}^{\max} = q n_d^{\max} v_C^- = q v_C^- \left(\frac{n_o^{\max} + \beta}{\delta} \right) \quad (A-36)$$

where β is given by (A-30) but here

$$\delta = 1 + \frac{d}{D_a} \left(\frac{\mu^+}{\mu^+ + \mu^-} \right) v_C^- \quad (A-37)$$

and $n_o^{\max} = \left(\frac{B}{2A} \right) \left[-1 + \sqrt{1 - \left(\frac{A}{B} \right) \left(\frac{C}{B} \right)} \right]$ (A-38)

where $A = v_E^- v_E^+ + (v_C^- v_E^+ / \delta),$ (A-39)

$$B = (\beta v_C^- v_E^+ / \delta) - Sd v_E^+ \quad (A-40)$$

and $C = - Sd v_E$ (A-41)

The critical current density J_{net}^C is the value of the net current density when the collector sheath changes sign and is given by

$$J_{\text{net}}^C = q \Gamma_{\text{net}}^C \quad (\text{A-42})$$

where $\Gamma_{\text{net}}^C = \frac{B}{2A} \left[-1 - \sqrt{1 - 4 \left(\frac{A}{B} \right) \left(\frac{C}{B} \right)} \right] . \quad (\text{A-43})$

In (A-43) the factors A, B, and C are

$$A = B_1 B_2 \alpha^2 + B_2 B_5 \alpha$$

$$B = -1 - B_2 B_3 \alpha - 2 B_1 B_2 \alpha \beta + B_5 - B_2 B_5 \beta$$

$$C = -B_3 + B_2 B_3 \beta + B_1 B_2 \beta^2$$

and

$$B_1 = v_E^-$$

$$B_2 = v_E^+ / v_E$$

$$B_3 = Sd$$

$$B_4 = v_C^- / (v_C^- - v_C^+)$$

and

$$\alpha = \left[\frac{1 + (v_C^+ d / D_a)}{v_C^- - v_C^+} + \left(\frac{\mu^+}{\mu^+ + \mu^-} \right) \left(\frac{d}{D_a} \right) \right]$$

and β is given by (A-30).

TABLE A-I. Definition of symbols.

SYMBOL	FORTRAN NAME	DEFINITION	VALUE
Fixed Constants			
e (= q)	Q	Electron charge	1.6021×10^{-19} coul.
π	PI		3.14159
k	KB	Boltzmann constant	1.3804×10^{-23} J/°K
m_e	ME	Mass of electron	9.1084×10^{-31} kg
Input Constants			
d , cm	D	Spacing	10^{-1}
S , $\text{cm}^{-3}\text{sec}^{-1}$	S	Ion generation rate	1.10×10^{16}
D_a , $\text{cm}^2\text{sec}^{-1}$	DA	Ambipolar diffusion coefficient	1.20×10^1
D_+ , $\text{cm}^2\text{sec}^{-1}$	DP	Ion diffusion coefficient	6.00×10^0
ν_E , A cm^{-2}	JRICH	Richardson emitter current	2.00
m_i , kg	MI	Mass of ion	6.6801×10^{-26}
μ_0^+ , $\text{cm}^2\text{volt}^{-1}\text{sec}^{-1}$	MUOIEN	Mobilities at 1 torr and 273°K	5.32×10^3
μ_0^- , $\text{cm}^2\text{volt}^{-1}\text{sec}^{-1}$	MUOEL		5.00×10^6
T_E , °K	TE	Emitter temperature	1700.
T_C , °K	TC	Collector temperature	900.
T_M , °K	TM	Mean gas temperature	1300.
p , torr	P	Gas pressure	1.0×10^2
Independent Variable			
J_{net} , A cm^{-2}	JNET	Net diode current	1.0×10^{-3}
Dependent Variable			
V , volt	VAPPL	Diode voltage (for $\phi_C = \phi_E$)	
V_E , volt	VOLTE	Emitter sheath potential difference	$V_E = (\Delta V)_E $
V_C , volt	VOLTC	Collector sheath potential difference	$V_C = (\Delta V)_C $
V_P , volt	VOLTP	Plasma potential difference	$V_P = (\Delta V)_P $
$J_{\text{net}}^{\text{min}}$, A cm^{-2}	JNET(NJ+1)	Saturation back current density	($V \rightarrow -\infty$)
J_{net}^C , A cm^{-2}	JNET(NJ+2)	Current density at which $V_C = 0$	
$J_{\text{net}}^{\text{max}}$, $\text{cm}^{-2}\text{sec}^{-1}$	JNET(NJ+3)	Saturation forward current density	($V \rightarrow +\infty$)
Γ_{net} , $\text{cm}^{-2}\text{sec}^{-1}$	GAMMA	$\Gamma_{\text{net}} = J_{\text{net}}/q$	
$\Gamma_{\text{net}}^{\text{min}}$, $\text{cm}^{-2}\text{sec}^{-1}$	GAMMIN	$\Gamma_{\text{net}}^{\text{min}} = J_{\text{net}}^{\text{min}}/q$	
Γ_{net}^C , $\text{cm}^{-2}\text{sec}^{-1}$	GAMMAC	$\Gamma_{\text{net}}^C = J_{\text{net}}^C/q$	
$\Gamma_{\text{net}}^{\text{max}}$, $\text{cm}^{-2}\text{sec}^{-1}$	GAMMAX	$\Gamma_{\text{net}}^{\text{max}} = J_{\text{net}}^{\text{max}}/q$	
$n(x)$, cm^{-3}	RNX	Plasma density at a distance x cm from the emitter	
n_0 , cm^{-3}	NO	Plasma density near emitter sheath	
n_d , cm^{-3}	ND	Plasma density near collector sheath	
v_E^+ , cm sec^{-1}	VEION	Average velocity of ions in plasma near emitter/4	
v_E^- , cm sec^{-1}	VEEL	Average velocity of electrons in plasma near emitter/4	
v_C^+ , cm sec^{-1}	VCION	Average velocity of ions in plasma near collector/4	
v_C^- , cm sec^{-1}	VCEL	Average velocity of electrons in plasma near collector/4	

APPENDIX B

TABLE B-I. Program listing and sample output.

```

C IAFTC MN5      LIST,REF,M94,XR7
C ELECTRON TRANSPORT PROGRAM (DIFFUSION ONLY)      JOB NO - AS9
C
C
C CALCULATES INTERNAL DIODE VOLTAGE (VAPPL =-VOLTE-(OR+)VOLTC+VOLTP)
C FOR INPUT VALUES OF NET CURRENT DENSITY (JNET, AMPS/CM**2)
C
C DIODE OUTPUT VOLTAGE WOULD BE = (VAPPL + CONTACT POTENTIAL)
C
C USES SUBROUTINE VFORIS FOR ELECTRON RETARDING COLLECTOR SHEATH
C USES SUBROUTINE VFORIL FOR ION RETARDING COLLECTOR SHEATH
C
C 1 NEUTRAL PLASMA (ION DENSITY = ELECTRON DENSITY = NX(X))
C 2 COLLISION DOMINATED PLASMA (ELECTRON MEAN FREE PATH
C GREATER THAN DEBYE LENGTH BUT LESS THAN DIODE SPACING)
C 3 DIFFUSION CONTROLLED PLASMA (RECOMBINATION LOSS = NIL)
C 4 UNIFORM ION GENERATION RATE (S)
C ASSUMES 5 COLLISION LESS SHEATHS
C 6 ELECTRON RICH EMITTER SHEATH (ION RETARDING TO PLASMA)
C 7 MAXWELLIAN DISTRIBUTION OF ELECTRON AND ION VELOCITIES
C 8 ELECTRON TEMP = ION TEMP = GAS TEMP = ELECTRODE TEMPS
C 9 PLASMA TEMP = MEAN ELECTRODE TEMP
C
C PRINTS 1 VAPPL VS JNET
C 2 JNET(MIN),JNET(MAX),JNET(VC=0)
C 3 NX(X) VS X FOR EACH JNET INPUT
C
C DIMENSION TITLE(24),JNET(50),VAPP(50)
C DIMENSION RNO(50),RND(50)
C COMMON /COM1/D,S,DA,DP,JRICH,Q,PI,KB,ME,MI,MUEL,MUION,
C 1VEEL,VCEL,VEION,VCION,KVEL,KVION,NU,TE,TC,TM,NJ,LD
C DOUBLE PRECISION P,MUION,MUEL,Q,PI,KB,ME,MI,TE,TC,TM,MUOION,MUOEL
C DOUBLE PRECISION D,S,DA,DP,JRICH,JNET,GAMMA,VAPPL,VAPP,NU
C DOUBLE PRECISION VEEL,VCEL,VEION,VCION,KVEL,KVION
C DOUBLE PRECISION NO,ND
C DOUBLE PRECISION NOC,NDC,VAPPC
C DOUBLE PRECISION RNO,RND,BETA,DELTA,AA,BB,CC,NOM,NDM,GAMMAX
C DOUBLE PRECISION NOMIN,NDMIN,GAMMIN
C DOUBLE PRECISION ALFA,B1,B2,B3,B5,A,B,C,GAMMAC
C NAMELIST/INPUT1/D,S,DA,DP,JRICH,MI,MUOION,MUOEL,TE,TC,TM,P
C NAMELIST/INPUT2/NJ,LD
C NAMELIST/NAM1/KVEL,KVION,MUION,MUEL,NU,VEEL,VCEL,VEION,VCION
C NAMELIST/NAM2/NOM,NDM,GAMMAX
C NAMELIST/NAM3/NOMIN,NDMIN,GAMMIN
C NAMELIST/NAM4/NOC,NDC,GAMMAC,VAPPC
C
C 20 READ (5,100)TITLE
C 100 FORMAT (12A6)
C 105 WRITE(6,110)TITLE
C 110 FORMAT (1H1,20X,12A6/21X,12A6)
C 120 READ (5,INPUT1)
C 125 WRITE(6,INPUT1)
C 130 DO 135 L=1,50
C 131 JNET(L)=0.0D0
C 134 RNO(L)=0.0D0
C 135 RND(L)=0.0D0
C 140 READ (5,INPUT2)
C 145 WRITE(6,INPUT2)

```

```

146 NJ3=NJ+3
150 READ (5,151)(JNET(N),N=1,NJ)
151 FORMAT(6D12.6)
160 WRITE (6,161)(JNET(N),N=1,NJ)
161 FORMAT(1H ,27HINPUT FOR NET CURRENT, AMPS/(5E20.8))

```

C

```

170 Q = 1.6021D-19
175 PI=3.14159 D0
180 KB=1.3804D-23
185 ME=9.1084D-31
190 KVEL =1.0D2*DSQRT((KB/ME)*(0.5D0/PI))
195 KVION=1.0D2*DSQRT ((KB/MI)*(0.5D0/PI))
200 MUION=MUOION/P
205 MUEL =MUOFL/P
210 NU=JRICHO
220 VEEL=KVEL*DSQRT(TE)
225 VCEL=KVEL*DSQRT(TC)
230 VEION=KVION*DSQRT(TE)
235 VCION=KVION*DSQRT(TC)
236 WRITE(6,NAM1)

```

C

```

240 RFTA=S*D*D/(2.0D0*DA)
250 DELTA=(1.0D0+(D/DA)*(MUION/(MUION+MUEL))*VCEL)
260 AA=(VEFL*VEION+(VCEL*VEION)/DELTA)
270 BB=(RFTA/DELTA)*VCEL*VEION-S*D*VEION
280 CC=-S*D*NU
290 NOM=(BB/(2.0D0*AA))*(-1.0D0+DSQRT(1.0D0-4.0D0*(AA/BB)*(CC/BB)))
300 NDM=(NOM+BETA)/DELTA
310 GAMMAX=NDM*VCEL
320 WRITE(6,NAM2)
330 RNO(NJ+3)=NOM
340 RND(NJ+3)=NDM
350 JNET(NJ+3)=Q*GAMMAX

```

C

```

360 DELTA =(1.0D0+(D/DA)*(MUEL/(MUION+MUEL))*VCION)
362 AA=VFEL*VEION
364 BB=(NU/DELTA)*VCION-S*D*VEION
366 CC=NU*(BETA/DELTA)*VCION-S*D*NU
368 NOMIN=(BB/(2.0D0*AA))*(-1.0D0+DSQRT(1.0D0-4.0D0*(AA/BB)*(CC/BB)))
370 NDMIN=(NOMIN+BETA)/DELTA
372 GAMMIN=-NDMIN*VCION
374 WRITE(6,NAM3)
376 RNO(NJ+1)=NOMIN
378 RND(NJ+1)=NDMIN
380 JNET(NJ+1)=Q*GAMMIN

```

C

```

400 ALFA=(1.0D0+VCION*D/DA)/(VCEL-VCION)+(MUION/(MUION+MUEL))*(D/DA)
410 B1=VFEL
420 B2=VEION/NU
430 B3=S*D
440 B5=VCEL/(VCEL-VCION)
450 A =B1*B2*ALFA*ALFA+B2*B5*ALFA
460 B =-1.0D0-B2*B3*ALFA -2.0D0*B1*B2*ALFA*BETA+B5-B2*B5*BETA
470 C = -B3+B2*B3*BETA +B1*B2*BETA*BETA
480 GAMMAC=(R/(2.0D0*A))*(-1.0D0-DSQRT(1.0D0-4.0D0*(A/B)*(C/B)))
482 WRITE (6,483) GAMMAC
483 FORMAT(1H ,24HCALCULATIONS FOR GAMMAC=E16.8,15H WHERE VC IS 0)
490 CALL VFORIS(GAMMAC,NO,ND,VAPPL)
500 NOC=NO

```

```

510 NDC=ND
520 VAPPC=VAPPL
530 WRITE(6,NAM4)
540 RNO(NJ+2)=NOC
550 RND(NJ+2)=NDC
560 VAPP(NJ+2)=VAPPC
570 JNET(NJ+2)=Q*GAMMAC

```

C

```

600 DO 800 N1=1,NJ
610 GAMMA=JNET(N1)/Q
614 IF(GAMMA-GAMMIN)616,616,620
616 VAPP(N1)=-1.0D10
618 GO TO 800
620 IF(GAMMA-GAMMAX)650,630,630
630 VAPP(N1)=1.0D10
640 GO TO 800
650 IF(GAMMA-GAMMAC)660,660,680
660 WRITE(6,661) JNET(N1)
661 FORMAT(1H ,23H CALCULATIONS FOR JNET =,E16.8,57H WHERE VC IS -VOLTC
6621(1E, ELECTRON RETARDING TO THE PLASMA))
665 CALL VFORIS(GAMMA,NO,ND,VAPPL)
670 GO TO 700
680 WRITE(6,681) JNET(N1)
681 FORMAT(1H ,23H CALCULATIONS FOR JNET =,E16.8,57H WHERE VC IS +VOLTC
6821(1E, ION RETARDING TO THE PLASMA))
685 CALL VFORIL(GAMMA,NO,ND,VAPPL)
700 RNO(N1)=NO
710 RND(N1)=ND
720 VAPP(N1)=VAPPL
800 CONTINUE

```

C

```

900 WRITE(6,910)
910 FORMAT(1H1,13H FINAL SUMMARY /1H0,13X,4H JNET,26X,2H NO,25X,2H ND,
911124X,5HVAPPL)
920 WRITE(6,930)(JNET(I),RNO(I),RND(I),VAPP(I),I=1,NJ3)
930 FORMAT(4D28,16)
950 GO TO 20
END

```

```

$IBFTC SUB6 LIST,REF,M94,XR7
SUBROUTINE VFORIS(GAMMA,NO,ND,VAPPL)

```

C

C

C

C

C

C

C

C

C

C

C

C

C

```

COMPUTATES INTERNAL VOLTAGE(VAPPL) FOR A GIVEN NET CURRENT (GAMMA)
FOR COLLECTOR SHEATH ELECTRON RETARDING TO THE PLASMA (VC=-VOLTC)

ALSO RETURNS PLASMA DENSITY AT EMITTER (NO) AND COLLECTOR (ND)
FOR EACH CALL THE PLASMA DENSITY (PNX) IS PRINTED OUT FOR LD STEPS
OF DISTANCE (X) ACROSS THE GAP (D)
ALSO PRINTED ARE VOLTE, VOLTC, AND PLASMA DROP (VOLTP)

```

```

COMMON /COM1/D,S,DA,DP,JRICH,Q,PI,KB,ME,MI,MUEL,MUION,
1VEEL,VCEL,VEION,VCION,KVEL,KVION,NU,TE,TC,TM,NJ,LD
DOUBLE PRECISION P,MUION,MUEL,Q,PI,KB,ME,MI,TE,TC,TM
DOUBLE PRECISION D,S,DA,DP,JRICH,JNET,GAMMA,VAPPL,VAPP,NU
DOUBLE PRECISION VEEL,VCEL,VEION,VCION,KVEL,KVION
DOUBLE PRECISION NO,ND
DOUBLE PRECISION X,RNX
DOUBLE PRECISION AN,BN,CN,DN,EN

```



```

DOUBLE PRECISION AVP,BVP,CVP,KVE,KVC,VOLTE,VOLTC,DVP1,DVP2
DOUBLE PRECISION VP1,VP21,VP22,VP2,VOLTP,VAPPL
NAMELIST/NAM6/NO,ND
NAMELIST/NAM7/KVE,KVC,VOLTE,VOLTC
NAMELIST/NAM8/VOLTP,VAPPL

```

C

```

100 AN=1.0D0 + D*VCION/DA
110 RN=((D*MUION*GAMMA)/(DA*(MUION+MUEL)))-S*D*D/(2.0D0*DA)
120 CN=VEEL*VEION + VEION*VCION/AN
130 DN=VEION*GAMMA-VEION*S*D-VEION*VCION*BN/AN+NU*VCION/AN
140 EN=-(((NU/AN)*VCION*RN)+(S*D*NU))
160 NO=-((0.5D0*DN/CN)*(1.0D0-DSQRT(1.0D0-(4.0D0*(EN/DN)/(DN/CN))))))
170 ND=NO/AN - RN/AN
180 WRITE(6,NAM6)
200 KVE=(GAMMA+NO*VEEL)/(NU+NO*VEION)
210 KVC=(VCION+GAMMA/ND)/VCEL
220 VOLTE=-(TE/1.16D4)*DLOG(KVE)
230 VOLTC=-(TC/1.16D4)*DLOG(KVC)
240 WRITE(6,NAM7)
250 X=0.0D0
252 XD=LD
254 XDD=D/XD
255 LD1=LD+1
256 WRITE(6,257) GAMMA
257 FORMAT(1H,18HNX VS X FOR GAMMA=,E16.8//,13X,1HX,27X,2HNX)
260 DO 290 L=1,LD1
270 RNX=NO-(S/(2.0D0*DA))*X*X-((MUION/(MUION+MUEL))*(GAMMA/DA)-
271 NO*VEION*KVE/DA)*X
275 X=X+XDD
280 WRITE(6,281) X,RNX
281 FORMAT(2D28.16)
290 CONTINUE
300 AVP=(S*D-ND*VCION-MUION*GAMMA/(MUION+MUEL))/DA
310 BVP=2.0D0*AVP*DA/S
320 CVP=2.0D0*NO*DA/S
400 DVP1=(DSQRT(BVP*BVP+4.0D0*CVP)-BVP)/2.0D0
410 DVP2=(DSQRT(BVP*BVP+4.0D0*CVP)+BVP)/2.0D0
420 VP1=(DP/MUION)*(DLOG(CVP+BVP*D-D*D)-DLOG(CVP))
430 VP21=(4.0D0*DP*GAMMA)/(S*(MUION+MUEL)*DSQRT(BVP*BVP+4.0D0*CVP))
440 VP22=DLOG((D+DVP1)/(DVP2-D))-DLOG(DVP1/DVP2)
500 VP2=VP21*VP22
510 VOLTP=VP1+VP2
520 VAPPL=-(VOLTE+VOLTC-VOLTP)
530 WRITE(6,NAM8)
600 RETURN
END

```

```

*IBFTC SUB7 LIST,REF,M94,XR7
SUBROUTINE VFORIL(GAMMA,NO,ND,VAPPL)

```

C
C
C
C
C
C
C
C
C
C
C
C

```

COMPUTATES INTERNAL VOLTAGE(VAPPL) FOR A GIVEN NET CURRENT (GAMMA)
FOR COLLECTOR SHEATH ION RETARDING TO THE PLASMA (VC=+VOLTC)

ALSO RETURNS PLASMA DENSITY AT EMITTER (NO) AND COLLECTOR (ND)
FOR EACH CALL THE PLASMA DENSITY (RNX) IS PRINTED OUT FOR LD STEPS
OF DISTANCE (X) ACROSS THE GAP (D)
ALSO PRINTED ARE VOLTE, VOLTC, AND PLASMA DROP (VOLTP)

```

```

COMMON /COM1/D,S,DA,DP,JRICH,Q,PI,KB,ME,MI,MUEL,MUION,
1VEEL,VCEL,VEION,VCION,KVEL,KVION,NU,TE,TC,TM,NJ,LD
DOUBLE PRECISION P,MUION,MUEL,Q,PI,KB,ME,MI,TE,TC,TM
DOUBLE PRECISION D,S,DA,DP,JRICH,JNET,GAMMA,VAPPL,VAPP,NU
DOUBLE PRECISION VEEL,VCEL,VEION,VCION,KVEL,KVION
DOUBLE PRECISION NO,ND
DOUBLE PRECISION X,RNX
DOUBLE PRECISION AN,BN,CN,DN,EN
DOUBLE PRECISION AVP,BVP,CVP,KVE,KVC,VOLTE,VOLTC,DVP1,DVP2
DOUBLE PRECISION VP1,VP21,VP22,VP2,VOLTP,VAPPL
• NAMELIST/NAM6/NO,ND
NAMELIST/NAM7/KVE,KVC,VOLTE,VOLTC
NAMELIST/NAM8/VOLTP,VAPPL

```

C

```

100 AN=1.0D0 + D*VCEL/DA
110 BN=-((D*MUEL*GAMMA)/(DA*(MUION+MUEL)))-S*D*D/(2.0D0*DA)
120 CN=VEEL*VEION+VEION*VCEL/AN
130 DN=-VEION*S*D-VEION*VCEL*BN/AN+NU*VCEL/AN
140 EN=-((NU/AN)*VCEL*BN+S*D*NU+GAMMA*NU)
160 NO=-((0.5D0*DN/CN)*(1.0D0-DSQRT(1.0D0-(4.0D0*(EN/DN)/(DN/CN))))
170 ND=NO/AN - BN/AN
180 WRITE(6,NAM6)
200 KVE=(GAMMA+NO*VEEL)/(NU+NO*VEION)
210 KVC=(S*D-NO*VEION*KVE)/(ND*VCION)
220 VOLTE=-(TE/1.16D4)*DLOG(KVE)
230 VOLTC=-(TC/1.16D4)*DLOG(KVC)
240 WRITE(6,NAM7)
250 X=0.0D0
252 XD=LD
254 XDD=D/XD
255 LD1=LD+1
256 WRITE(6,257) GAMMA
257 FORMAT(1H,18HX VS X FOR GAMMA=.E16,B// 13X,1HX,27X,2HNX)
260 DO 290 L=1,LD1
270 RNX=NO-(S/(2.0D0*DA))*X*X+((MUEL/(MUION+MUEL))*(GAMMA/DA)-
2711(NU*(KVE/DA)-NO*(VEEL/DA)))*X
275 X=X+XDD
280 WRITE(6,281) X,RNX
281 FORMAT(2D28.16)
290 CONTINUE
300 AVP=((NO*VEION*KVE)/DA-(MUION*GAMMA)/(DA*(MUION+MUEL)))
310 BVP=2.0D0*AVP*DA/S
320 CVP=2.0D0*NO*DA/S
400 DVP1=(DSQRT(BVP*BVP+4.0D0*CVP)-BVP)/2.0D0
410 DVP2=(DSQRT(BVP*BVP+4.0D0*CVP)+BVP)/2.0D0
420 VP1=(DP/MUION)*(DLOG(CVP+BVP*D-D*D)-DLOG(CVP))
430 VP21=(4.0D0*DP*GAMMA)/(S*(MUION+MUEL)*DSQRT(BVP*BVP+4.0D0*CVP))
440 VP22=DLOG((D+DVP1)/(DVP2-D))-DLOG(DVP1/DVP2)
500 VP2=VP21*VP22
510 VOLTP=VP1+VP2
520 VAPPL=-(VOLTE-VOLTC-VOLTP)
530 WRITE(6,NAM8)
600 RETURN
END

```

TABLE B-II. Sample of code output.

```

      RUN 10.1          V VS I      NE-AP
      JNET*D+03 = 1.0,2.5,5.0,10.0,70.0,120.0

$INPLT1
D      =      0.999999999999997D-01,
S      =      0.110000000000000D 17,
CA     =      0.120000000000000D 02,
DP     =      0.599999999999998D 01,
JRICH  =      0.200000000000000D 01,
MI     =      0.668009999999997D-25,
MUOICH =      0.531999999999999D 04,
MUOEL  =      0.500000000000000D 07,
TE     =      0.170000000000000D 04,
TC     =      0.899999999999998D 03,
TM     =      0.130000000000000D 04,
P      =      0.100000000000000D 03,
$ ENC
$INPLT2
NJ      =      6,
LD      =      10,
$ ENC
INPLT FOR NET CURRENT, AMPS
      0.99999999E-03      0.25000000E-02      0.49999999E-02
      0.99999999E-02      0.69999999E-01      0.12000000E 00

$NAME1
KVEL   =      0.1553072312065078D 06,
KVICH  =      0.5734839166530672D 03,
MUICH  =      0.531999999999998D 02,
MUOEL  =      0.500000000000000D 05,
NU     =      0.1248361525497784D 20,
VEEL   =      0.6403481186866548D 07,
VCEL   =      0.4655216936195234D 07,
VEICH  =      0.2364534762953511D 05,

```

VCICN = 0.1720451749959202D 05,

\$ END

\$NAM2

NOM = 0.2623927653724624D 12,

NDM = 0.1146434030414110D 12,

GAMMAX = 0.5341484850735982D 18,

\$ END

\$NAM3

NOMIN = 0.2087541650347371D 12,

NDMIN = 0.3322822214686861D 11,

GAMMIN = -0.5716755254061320D 15,

\$ END

CALCULATIONS FOR GAMMAC= C.12028628E 18 WHERE VC IS 0

\$NAME

NO = 0.2230884001470300D 12,

NC = 0.2591252780274686D 11,

\$ END

\$NAM7

KVE = 0.1240165152583116D 00,

KVC = 0.9999999999999957D 00,

VOLTE = 0.3059033542201612D 00,

VOLTC = 0.3187105751725670D-15,

\$ END

AX VS X FOR GAMMA= C.12028628E 18

X	AX
C.9999999852897903D-C2	0.2230884001470300D 12
C.1999999978579581D-C1	0.6158708091967041D 12
C.2999999967869371D-C1	C.9169865535432500D 12
C.3999999957159161D-C1	0.1126435633186668D 13
C.4999999946448952D-C1	C.1244218048126957D 13
C.5999999935736741D-C1	0.1270333758364118D 13
C.6999999925028531D-C1	C.1204782883898152D 13
0.7999999914318322D-01	0.1047565304729056D 13
C.8999999903608111D-C1	0.7986810608568327D 12
C.9999999892897903D-C1	0.4581301522814811D 12
C.1099999988218769D 00	0.2591257900300970 11

\$NAME

VOLTP = C.17022837414457990 00,

VAPPL = -0.12556496007558150 00,

\$ ENC

\$NAM4

NCC = 0.22308840C1470300D 12,

NCC = 0.2591252780274686D 11,

GAMMAC = C.12028627586C1466D 18,

VAPPC = -0.1255649800755815D 00,

\$ ENC

CALCULATIONS FOR JNET = 0.9999999E-03 WHERE VC IS -VOLTC(IE,
ELECTRON RETARDING TO THE PLASMA)

\$NAM6

NC = 0.2096586393923920D 12,

ND = 0.3281619890653208D 11,

\$ ENC

\$NAM7

KVE = 0.1080016902132138D 00,

KVC = 0.4451597703279608D-01,

VOLTE = 0.3261667485481592D 00,

VOLTC = 0.2414410696398514D 00,

\$ ENC

NX VS X FOR GAMMA= 0.62418076E 16

X	NX
0.5555599852897903D-02	0.2096586393923920D 12
0.199999976575581D-01	0.6044743916061309D 12
0.2555599567869271D-01	C.9076234791167418D 12
0.3555599557159161D-01	0.1119105901924224D 13
0.455559946448552D-01	0.1238921660028579D 13
0.555559935738741D-01	0.1267070753429805D 13
0.655559925028531D-01	0.1203553182127903D 13
0.755559914318322D-01	0.1048368546122872D 13
0.855559903608111D-01	0.8015180454147135D 12
0.955559892897903D-01	0.4530004800034264D 12
0.10555988218769D 00	0.3281624998901172D 11

\$NAME

VOLTP = -0.1881487268279062D 00,

VAPPL = -0.7557565450159167D 00,

\$ ENC

NOTE: Output for intermediate current values were deleted.

CALCULATIONS FOR JNET = 0.69999999E-01 WHERE VC IS +VOLTAGE,
ION RETARDING TO THE PLASMA)

\$NAME

NO = 0.2544126784845697D 12,

NO = 0.9379932675301916D 11,

\$ END

\$NAME7

KVE = 0.165421488072915D 00,

KVC = 0.6498927782101688D-01,

VCLTE = 0.263684448380776D 00,

VCLTC = 0.212084455289980D 00,

\$ END

AX VS X FOR GAMMA= 0.43692653E 18

X	AX
0.9999999892897903D-02	0.2544126784845697D 12
0.1999999978579581D-01	0.6503513395562595D 12
0.2999999967869371D-01	0.9556233359248213D 12
0.3999999957159161D-01	0.1168728667590255D 13
0.4999999946448952D-01	0.1290167334552560D 13
0.5999999935736741D-01	0.1319939336811738D 13
0.6999999925028531D-01	0.1253044674367786D 13
0.7999999914318322D-01	0.1104483347220707D 13
0.8999999903608111D-01	0.8592553553704992D 12
0.9999999892897903D-01	0.522360698171636D 12
0.1099999988218769D 00	0.9379937756069969D 11

\$NAME

VCLTP = 0.1115613985596936D 01,

VAPPL = 0.1064013996506838D 01,

\$ END

FINAL SUMMARY 10.1

JNET

0.1000000000000000-02
 0.2500000000000000-02
 0.5000000000000000-02
 0.1000000000000000-01
 0.6500000000000000-01
 0.1200000000000000 00
 -0.91588136566156390-04
 0.19271064255554080-01
 0.85575928793641150-C1

NO

0.20965863339239200 12
 0.21083402334949530 12
 0.21276171272109120 12
 0.21650562189422330 12
 0.25441267348456970 12
 0.0000000000000000-38
 0.20879416503473710 12
 0.22306840014703000 12
 0.26239276537246240 12

ND

0.32816198906532080 11
 0.32249932591955200 11
 0.31305938710004830 11
 0.29417178840998860 11
 0.93799326753019160 11
 0.0000000000000000-38
 0.33228222146868610 11
 0.25912527802746860 11
 0.11464340304141100 12

VAPPL

-0.75575654501591670 00
 -0.65650335616197850 00
 -0.55036162062915900 00
 -0.38920917413810680 00
 0.10640139965068380 01
 0.1000000000000000 11
 -0.0000000000000000-19
 -0.13556498007558150 00
 -0.0000000000000000-19

Job No. = AS9

TABLE B-III. Sample of input data sheet.

IBM DATA SHEET		IDENTIFICATION NUMBER	
1	2	3	4
1	2	3	4
5	6	7	8
9	10	11	12
13	14	15	16
17	18	19	20
21	22	23	24
25	26	27	28
29	30	31	32
33	34	35	36
37	38	39	40
41	42	43	44
45	46	47	48
49	50	51	52
53	54	55	56
57	58	59	60
61	62	63	64
65	66	67	68
69	70	71	72
73	74	75	76
77	78	79	80
RUN 10.11 V VS I ME-AR			
NMET#D+P3 = 1.0, 2.5, 5.0, 10.0, 70.0, 120.0			
INPUT1 D=1.00D-01, S=1.10D16, DA=1.20D1, DP=0.60D1, JRICW=2.00D0			
MI=6.68D1D-26, MUOIEW=5.320D3, MUDEL=5.000D6			
TE=1.700D3, TC=9.00D2, TM=1.300D3, P=1.000D2			
\$IMPVTZ NJ=4, LD=10			
1.0D-03 2.5D-03 5.0D-03 1.0D-02 7.0D-02 1.2D-01			

PUBLICATION

1. C. B. Leffert, D. B. Rees, and F. E. Jamerson, "Electron Density Maximization in a Penning Gas Mixture Ionized by Fission Fragments", Physics Letters, 22, 423 (1966).
2. Charles B. Leffert, David B. Rees, and Frank E. Jamerson, "Noble Gas Plasma Produced by Fission Fragments", J. of Appl. Phys., Vol. 37, No. 1, January 1966.

UNCLASSIFIED

Security Classification

DOCUMENT CONTROL DATA - R&D

(Security classification of title, body of abstract and indexing annotation must be entered when the overall report is classified)

1. ORIGINATING ACTIVITY (Corporate author) Research Laboratories, General Motors Corporation 12 Mile and Mound Roads, Warren, Michigan 48090		2a. REPORT SECURITY CLASSIFICATION UNCLASSIFIED	
		2b. GROUP N A	
3. REPORT TITLE INVESTIGATIONS ON THE DIRECT CONVERSION OF NUCLEAR FISSION ENERGY TO ELECTRICAL ENERGY IN A PLASMA DIODE.			
4. DESCRIPTIVE NOTES (Type of report and inclusive dates) Annual Report No. 7 - November 1, 1965 to October 31, 1966			
5. AUTHOR(S) (Last name, first name, initial) Leffert, Charles B. Rees, David B.			
6. REPORT DATE October 31, 1966	7a. TOTAL NO. OF PAGES 88	7b. NO. OF REFS 25	
8a. CONTRACT OR GRANT NO. Nonr-3109(00)	9a. ORIGINATOR'S REPORT NUMBER(S) GMR - 615		
b. PROJECT NO. 099-345	9b. OTHER REPORT NO(S) (Any other numbers that may be assigned this report) None		
c.			
d.			
10. AVAILABILITY/LIMITATION NOTICES Qualified requesters may obtain copies of this report from DDC.			
11. SUPPLEMENTARY NOTES None		12. SPONSORING MILITARY ACTIVITY Office of Naval Research (Zip Code: 20360) Power Branch (Code 429) Department of the Navy, Washington, D.C.	
13. ABSTRACT Inpile microwave measurements of electron density in neon-argon and argon-cesium plasmas generated by fission fragments are compared with values of electron density predicted from a reaction kinetics theory. The main purpose of the comparison is to assess the validity of a theory designed to describe the dominant production and loss processes in noble gas-cesium thermionic converters over a wide range of conditions. For the neon-argon system the measured and predicted values were in good agreement; the highest electron density was $1.0 \times 10^{12} \text{cm}^{-3}$ at full reactor power ($\phi = 1.44 \times 10^{13} \text{cm}^{-2} \text{sec}^{-1}$). For the argon-cesium system the agreement between theory and experiment was less satisfactory. The highest measured electron density at full reactor power was $2.3 \times 10^{12} \text{cm}^{-3}$ —approximately twice the computed value, and this maximum in the curve of electron density vs the ratio of Cs/Ar occurred at a ratio ($\sim 2 \times 10^{-5}$) much lower than that predicted ($\sim 3 \times 10^{-4}$). Furthermore the electron density was found to be extremely dependent upon the temperature of the cavity walls. No satisfactory explanation has yet been found for this behavior. Favorable electron transport properties are expected to make the fission-fragment-generated argon-cesium plasma a good candidate for use in a nuclear thermionic converter. Theoretical transport properties are reported for this plasma when the major ion loss mechanism is ambipolar diffusion to the thermionic diode electrodes. The theoretical model is being expanded to include volume loss of the ions.			

14. KEY WORDS	LINK A		LINK B		LINK C	
	ROLE	WT	ROLE	WT	ROLE	WT
1. Direct energy conversion 2. Thermionics 3. Gaseous electronics 4. Plasma physics						

INSTRUCTIONS

1. ORIGINATING ACTIVITY: Enter the name and address of the contractor, subcontractor, grantee, Department of Defense activity or other organization (*corporate author*) issuing the report.

2a. REPORT SECURITY CLASSIFICATION: Enter the overall security classification of the report. Indicate whether "Restricted Data" is included. Marking is to be in accordance with appropriate security regulations.

2b. GROUP: Automatic downgrading is specified in DoD Directive 5200.10 and Armed Forces Industrial Manual. Enter the group number. Also, when applicable, show that optional markings have been used for Group 3 and Group 4 as authorized.

3. REPORT TITLE: Enter the complete report title in all capital letters. Titles in all cases should be unclassified. If a meaningful title cannot be selected without classification, show title classification in all capitals in parenthesis immediately following the title.

4. DESCRIPTIVE NOTES: If appropriate, enter the type of report, e.g., interim, progress, summary, annual, or final. Give the inclusive dates when a specific reporting period is covered.

5. AUTHOR(S): Enter the name(s) of author(s) as shown on or in the report. Enter last name, first name, middle initial. If military, show rank and branch of service. The name of the principal author is an absolute minimum requirement.

6. REPORT DATE: Enter the date of the report as day, month, year, or month, year. If more than one date appears on the report, use date of publication.

7a. TOTAL NUMBER OF PAGES: The total page count should follow normal pagination procedures, i.e., enter the number of pages containing information.

7b. NUMBER OF REFERENCES: Enter the total number of references cited in the report.

8a. CONTRACT OR GRANT NUMBER: If appropriate, enter the applicable number of the contract or grant under which the report was written.

8b, 8c, & 8d. PROJECT NUMBER: Enter the appropriate military department identification, such as project number, subproject number, system numbers, task number, etc.

9a. ORIGINATOR'S REPORT NUMBER(S): Enter the official report number by which the document will be identified and controlled by the originating activity. This number must be unique to this report.

9b. OTHER REPORT NUMBER(S): If the report has been assigned any other report numbers (*either by the originator or by the sponsor*), also enter this number(s).

10. AVAILABILITY/LIMITATION NOTICES: Enter any limitations on further dissemination of the report, other than those imposed by security classification, using standard statements such as:

(1) "Qualified requesters may obtain copies of this report from DDC."

(2) "Foreign announcement and dissemination of this report by DDC is not authorized."

(3) "U. S. Government agencies may obtain copies of this report directly from DDC. Other qualified DDC users shall request through _____."

(4) "U. S. military agencies may obtain copies of this report directly from DDC. Other qualified users shall request through _____."

(5) "All distribution of this report is controlled. Qualified DDC users shall request through _____."

If the report has been furnished to the Office of Technical Services, Department of Commerce, for sale to the public, indicate this fact and enter the price, if known.

11. SUPPLEMENTARY NOTES: Use for additional explanatory notes.

12. SPONSORING MILITARY ACTIVITY: Enter the name of the departmental project office or laboratory sponsoring (*paying for*) the research and development. Include address.

13. ABSTRACT: Enter an abstract giving a brief and factual summary of the document indicative of the report, even though it may also appear elsewhere in the body of the technical report. If additional space is required, a continuation sheet shall be attached.

It is highly desirable that the abstract of classified reports be unclassified. Each paragraph of the abstract shall end with an indication of the military security classification of the information in the paragraph, represented as (TS), (S), (C), or (U).

There is no limitation on the length of the abstract. However, the suggested length is from 150 to 225 words.

14. KEY WORDS: Key words are technically meaningful terms or short phrases that characterize a report and may be used as index entries for cataloging the report. Key words must be selected so that no security classification is required. Identifiers, such as equipment model designation, trade name, military project code name, geographic location, may be used as key words but will be followed by an indication of technical context. The assignment of links, rules, and weights is optional.